PERGAMON

International Journal of Solids and Structures 38 (2001) 3689–3717

INTERNATIONAL JOURNAL OF SOLIDS and STRUCTURES

www.elsevier.com/locate/ijsolstr

A refined analysis of the effective elasticity tensor for general cellular sandwich cores

Jörg Hohe *, Wilfried Becker

Institut für Mechanik und Regelungstechnik, Universität Siegen, Paul-Bonatz-Str. 9-11, D-57068 Siegen, Germany

Received 24 January 2000; in revised form 29 May 2000

Abstract

The aim of the present study is the determination of the components of the effective elasticity tensor for two-dimensional cellular sandwich cores in consideration of core face sheet constraints. The microstructure is homogenized by means of a strain-energy based RVE concept assuming that strain states, which are equivalent on the macroscopic level, lead to equal strain energy in a representative volume element whether the real microstructure or the quasi-homogeneous "effective" medium is considered. The strain energy can be evaluated analytically if the cellular structure is decomposed into the individual cell wall elements, and assumptions are made for the displacement field of each cell wall. The displacement field of the core is approximated by a weighted superposition of the displacement field of the unconstrained core and an extension of the displacements of the face sheets into the core region. Since the approach is based on a kinematically admissible strain field in conjunction with the principle of minimum strain energy, the results provide rigorous Voigt type bounds for the effective normal and shear moduli. In general, a good agreement of the analytical results and the results of a finite element analysis is observed.

Keywords: Elasticity; Homogenization; Honeycomb structure; Mechanical property; Modelling; Sandwich materials

1. Introduction

Structural sandwich panels are important elements of lightweight construction especially in aerospace applications. The typical structural sandwich panel consists of three layers: Two high-density face sheets are bonded to a low-density core (Fig. 1). Two-dimensional cellular structures are common core materials. Within this principle of construction, the core has to keep the face sheets at the desired distance and carry the transverse shear loads. Advantage of sandwich structures is that large bending stiffness values in conjunction with very low specific weight are obtained.

For reasons of numerical efficiency, the analysis of sandwich plates and shells during the design process is performed in terms of effective properties rather than by direct consideration of the cellular microstructure.

* Corresponding author. Tel.: +49-271-740-4642; fax: +49-271-740-2461.
E-mail address: hohe@imr-sun4.fb5.uni-siegen.de (J. Hohe).

0020-7683/01/$ - see front matter
PII: S0020-7683(00)00246-8

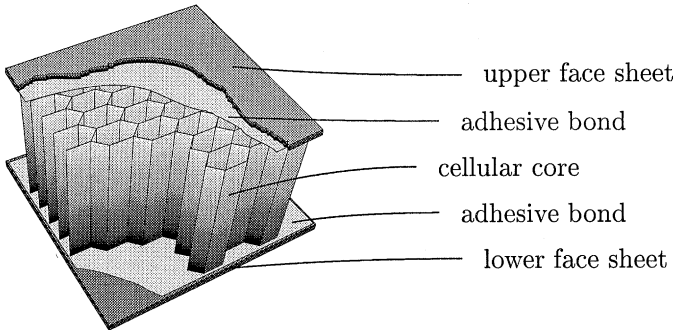

Fig. 1. Structural sandwich panel.

Therefore, the cellular structure has to be replaced by a quasi-homogeneous "effective" medium. The properties of the effective medium have to be determined in such a way that the mechanical behaviour of both the cellular structure and the effective medium are equivalent at the macroscopic level.

The pioneering work on determination of effective properties for two-dimensional cellular sandwich cores was performed by Kelsey et al. (1958) as well as by Chang and Ebcioglu (1961) who considered the transverse shear moduli of regular hexagonal honeycomb cores. Due to the importance of structural sandwich panels for the design of lightweight structures, numerous studies regarding the effective properties are available in the literature. Most of these studies are concerned with hexagonal as well as other cell geometries which are orthotropic on the effective level (Gibson et al., 1982; Warren and Kraynik, 1987; Gibson and Ashby, 1997; Torquato et al., 1998; Meraghni et al., 1999). A generalization to the non-orthotropic case has been provided by the authors of the present study (Hohe and Becker, 1999, 2000). In these studies, a general analytical scheme is presented, which enables the determination of the components of the effective elasticity tensor for two-dimensional cellular materials with general cell geometry consisting of straight and curved cell walls.

Most of the studies available in the literature consider the case of the free core which is not constrained by the face sheets. Nevertheless, the modes of deformation of the unconstrained core and the face sheets are in most cases incompatible (Fig. 2). In a sufficient distance to the face sheets, the displacement field of the core can be described approximately by the displacement field of the free core. In the vicinity of the face sheets, a transition in the mode of deformation from the mode associated with the unconstrained core to the mode associated with the face sheets occurs. In this transition zone, additional strain energy is stored. Thus, a significant increase in the effective moduli of the constrained core in comparison to the unconstrained situation may occur. This effect was studied by Grediac (1993) in a finite element analysis considering the transverse shear moduli of hexagonal cores. Becker (1998) provided an analytical approach for the in-plane normal components of the effective elasticity tensor for regular hexagonal cores. In this paper, this approach is generalized to all components of the elasticity tensor as well as to two-dimensional cellular cores with arbitrary cell geometry.

For homogenization of composite and cellular materials, several approaches have been developed. Most studies use a simple redistribution of stress and strain on the surfaces of a representative volume element (Kelsey et al., 1958; Chang and Ebcioglu, 1961; Gibson and Ashby, 1997). An approach based on energetic considerations has been provided by Bishop and Hill (1951) and Hill (1984). In the analysis of non-linear composites, a similar approach has been used by Ponte Castaneda and Suquet (1998). On the contrary, rigorous mathematical theories such as the variational principles of Hashin and Shtrikman (1962) or perturbation theory based approaches (Sanchez-Palencia, 1980; Bakhvalov and Panasenko, 1989) can be

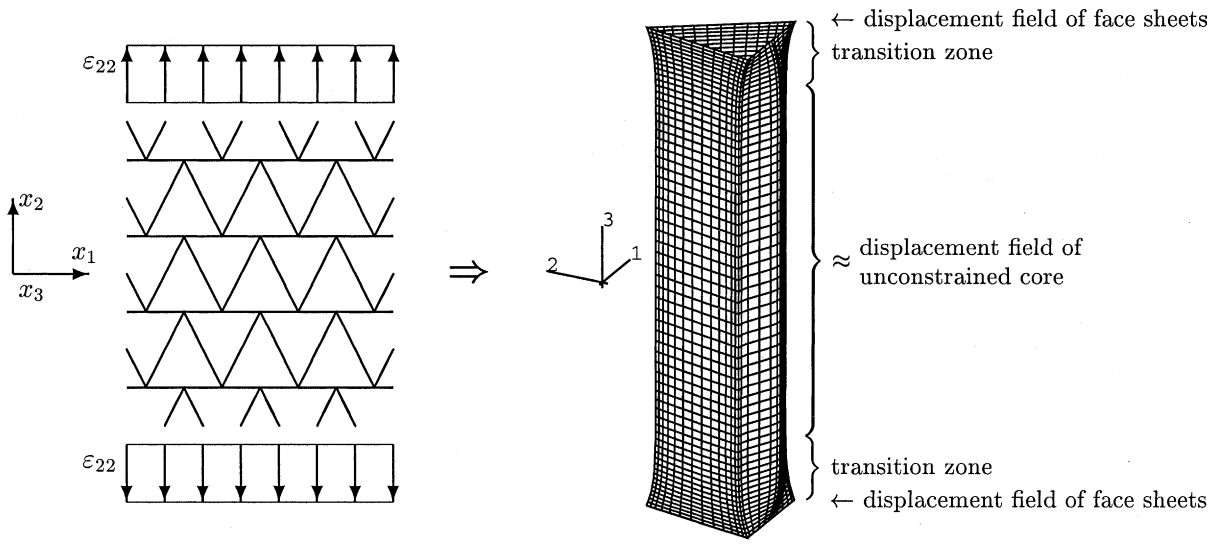

Fig. 2. Core face sheet deformation constraint.

employed. In the present study, the homogenization of the microstructure is performed by means of a strain energy based concept. Within this scheme, equivalence of the mechanical behaviour of the cellular structure and the homogenized effective medium is assumed, if the strain energy in a representative volume element is equal whether the cellular structure or the effective medium is considered, provided that the representative volume element is subjected to a strain state which for both cases is equal in an average sense.

The strain energy is evaluated analytically for the limiting cases of an unconstrained core and a core which is deformed according to the mode of deformation of the face sheets. For the case of the unconstrained core, a matrix scheme based on standard Euler–Bernoulli beam theory is employed to determine the displacement field of the cell walls. In the second case, the displacement field of the face sheets is extended into the core region. In a refined approach, the displacement field of the core in the assembled situation is approximated by a weighted superposition of the displacement fields in both the limit cases. The free parameters in the weight function are determined by the application of the principle of minimum strain energy.

In a comparative analysis, the finite element method is used for the determination of strain energy. Both the approaches are found to agree well in three examples considering commercial sandwich core geometries especially in case of the transverse properties which are the most important properties from the technological point of view. Since the analytical approach is based on a kinematically admissible displacement and strain field, the analytical scheme provides rigorous Voigt type bounds (Voigt, 1889; Hill, 1952) for the effective elastic moduli of the cellular sandwich core.

2. Strain energy based concept for homogenization

Consider a mechanical body Ω according to Fig. 3 with a characteristic dimension Y. The body Ω is bounded by the external boundary $\Gamma = \Gamma_u \cup \Gamma_t$, where either displacements u_i^0 or tractions T_i^0 are prescribed. In addition to the surface tractions T_i^0, Ω is subjected to body forces f_i^0. The body Ω is assumed to consist of a cellular material with periodic microstructure. For analysis, Ω has to be replaced by a similar

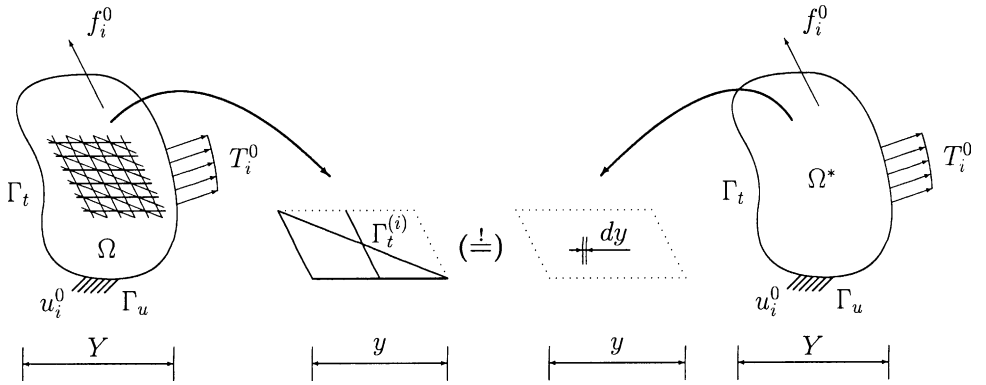

Fig. 3. Representative volume element.

body Ω^* with the same external boundaries Γ_u and Γ_t subjected to the same external boundary conditions. The body Ω^* is assumed to consist of a homogeneous medium (the "effective" medium) with yet unknown properties.

Since the effective material behaviour does not depend on the external shape and loading of Ω, a representative volume element for the microstructure of Ω and a corresponding volume element consisting of the effective medium are considered for the determination of the properties of the effective medium. The characteristic dimension of the representative volume element is y with $Y \gg y \gg \mathrm{d}y$, where $\mathrm{d}y$ is an infinitesimal length scale. The properties of the effective medium have to be determined in such a way that the mechanical behaviour of both volume elements is equivalent at the macroscopic level.

A criterion for the equivalence of both the volume elements can be defined by the condition that equal strain energy in both volume elements has to result if both volume elements are deformed by macroscopically equivalent strain states ε_{ij} and ε_{ij}^*, respectively. Thus, the condition

$$\overline{w} = \frac{1}{V}\int_V w(\varepsilon_{ij})\mathrm{d}V = \frac{1}{V}\int_{V^*} w^*(\varepsilon_{ij}^*)\mathrm{d}V^* = \overline{w}^* \tag{1}$$

has to be satisfied, where the strain energy density in the volume elements is denoted by w and w^*, respectively, while $V = V^*$ denotes the volume of the representative volume elements. Macroscopic (effective) field quantities are denoted by bars.

According to Bishop and Hill (1951), macroscopic equivalence of the strain states ε_{ij} and ε_{ij}^* is assumed, if the volume average of both strain states with respect to the representative volume element is equal:

$$\overline{\varepsilon}_{ij} = \frac{1}{V}\int_V \varepsilon_{ij}\,\mathrm{d}V = \frac{1}{V}\int_{V^*} \varepsilon_{ij}^*\,\mathrm{d}V^* = \overline{\varepsilon}_{ij}^*. \tag{2}$$

With a linear constitutive relation in a local formulation

$$\overline{\sigma}_{ij} = \overline{C}_{ijkl}\overline{\varepsilon}_{kl} \tag{3}$$

with the stress tensor $\overline{\sigma}_{ij}$ being assumed for the effective medium, the components $\overline{C}_{ijkl}$ of the effective elasticity tensor are given by the second partial derivatives of the strain energy density with respect to the components of the strain tensor:

$$\overline{C}_{ijkl} = \frac{\partial^2 \overline{w}^*}{\partial \overline{\varepsilon}_{ij}^* \partial \overline{\varepsilon}_{kl}^*} = \frac{\partial^2 \overline{w}}{\partial \overline{\varepsilon}_{ij}^* \partial \overline{\varepsilon}_{kl}^*}. \tag{4}$$

If the differentiation in Eq. (4) is performed numerically, the following expression for the components of the effective elasticity tensor is obtained:

$$\overline{C}_{ijkl} = \begin{cases} 2\overline{w}(\overline{\varepsilon}_{(ij)})\frac{1}{\overline{\varepsilon}^2_{(ij)}} & \text{if } i=j \text{ and } k=l \text{ and } i=k, \\ \frac{1}{2}\overline{w}(\overline{\varepsilon}_{(ij)})\frac{1}{\overline{\varepsilon}^2_{(ij)}} & \text{if } i\neq j \text{ and } k\neq l \text{ and } i=k \text{ and } j=l, \\ \left(\overline{w}(\overline{\varepsilon}_{(ij)},\overline{\varepsilon}_{(kl)}) - \overline{w}(\overline{\varepsilon}_{(ij)}) - \overline{w}(\overline{\varepsilon}_{(kl)})\right)\frac{1}{\overline{\varepsilon}_{(ij)}\overline{\varepsilon}_{(kl)}} & \text{if } i=j \text{ and } k=l \text{ and } i\neq k, \\ \frac{1}{4}\left(\overline{w}(\overline{\varepsilon}_{(ij)},\overline{\varepsilon}_{(kl)}) - \overline{w}(\overline{\varepsilon}_{(ij)}) - \overline{w}(\overline{\varepsilon}_{(kl)})\right)\frac{1}{\overline{\varepsilon}_{(ij)}\overline{\varepsilon}_{(kl)}} & \text{if } i\neq j \text{ and } k\neq l \text{ and } (i\neq k \text{ or } j\neq l), \\ \frac{1}{2}\left(\overline{w}(\overline{\varepsilon}_{(ij)},\overline{\varepsilon}_{(kl)}) - \overline{w}(\overline{\varepsilon}_{(ij)}) - \overline{w}(\overline{\varepsilon}_{(kl)})\right)\frac{1}{\overline{\varepsilon}_{(ij)}\overline{\varepsilon}_{(kl)}} & \text{if } i=j \text{ and } k\neq l, \end{cases} \tag{5}$$

where $\overline{w}(\overline{\varepsilon}_{(ij)},\overline{\varepsilon}_{(kl)})$ denotes the strain energy density for a reference strain state, where only $\overline{\varepsilon}_{ij}$ and $\overline{\varepsilon}_{kl}$ have non-zero values. Indices in parentheses mean that no summation has to be performed. Homogeneous reference strain states $\overline{\varepsilon}_{ij}$ can be used with no loss in generality, since the material properties according to Eq. (3) do not depend on the strain state. The same result as Eq. (5) is obtained, if the equation $\overline{w} = \overline{\sigma}_{ij}\overline{\varepsilon}_{ij}/2$ for the strain energy density in the case of local linear elasticity is evaluated for the mentioned reference strain states and solved for $\overline{C}_{ijkl}$.

Thus, the determination of the effective properties can be performed by means of the following procedure:

1. Apply all 21 homogeneous strain states, where only one or two components of the effective strain tensor $\overline{\varepsilon}_{ij}$ have non-zero values to a representative volume element for the microstructure of Ω providing that Eq. (2) is satisfied.
2. Compute the average strain energy density for all reference strain states according to Eq. (1).
3. Compute the components $\overline{C}_{ijkl}$ of the effective elasticity tensor by means of Eq. (5).

Within this concept, the evaluation of the average strain energy density $\overline{w}$ for the representative volume element can be performed either analytically or numerically.

3. Analytical determination of the strain energy

3.1. Decomposition of the representative volume element

The first step for the application of the concept for homogenization presented in Section 2 consists in identification of a representative volume element for the given cellular structure. An appropriate representative volume element for general two-dimensional cellular media is presented in Fig. 4. Irrespective of the microstructure, a parallelogram-shaped volume element set up by the parameters a, b and c according to Fig. 4 can always be found. For the analysis of the volume element, a cartesian coordinate system x_i is introduced, where x_1 is orientated along the base of the parallelogram-shaped volume element and x_3 is the direction transverse to the sandwich plane.

For evaluation of the strain energy, the representative volume element is decomposed into the individual cell wall elements (Fig. 5). Thus, the strain energy of the entire volume element can be determined by the sum of the strain energies of the cell wall elements. The displacement field of the cell wall elements and subsequently the strain energy of the cell wall elements can be expressed in terms of the deflections of the cell wall ends (subsequently termed "nodal points"). The following notation is introduced: The displacement of nodal point i in x_j-direction is denoted by $v_{(i)j}$, while $\Delta\varphi_{(i)}$ denotes the rotation at nodal point i with respect to the x_3-axis. For description of the displacement field of the individual cell walls, local systems $\tilde{x}_i$

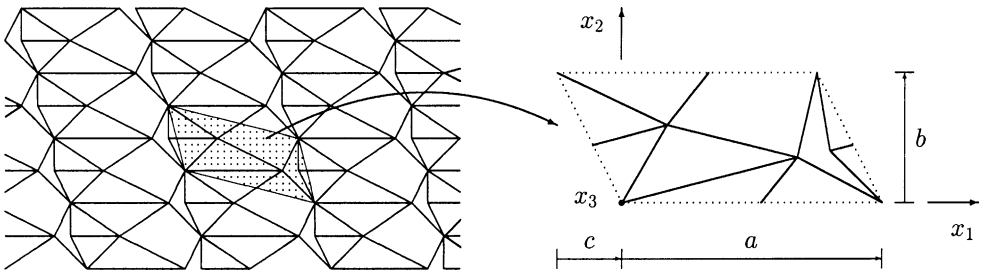

Fig. 4. Representative volume element for general cellular sandwich cores.

are introduced, where $\tilde{x}_1$ is the longitudinal direction, $\tilde{x}_2$ is the direction normal to the cell wall plane and $\tilde{x}_3 = x_3$ (Fig. 6). All quantities with respect to the local system are marked by a tilde.

The nodal points of the representative volume element are numbered according to Fig. 5. The numbering starts with corner nodes 1 and 2 at the left-hand side of the representative volume element followed by all pairs of corresponding nodes i and $i+1$ along the x_1-parallel surfaces up to the corner nodes p and $p+1$ at the right-hand side of the volume element. Subsequently, all pairs of corresponding nodes j and $j+1$ along the inclined surfaces are numbered starting with the pair $p+2$ and $p+3$ next to nodes 1 and p, and ending

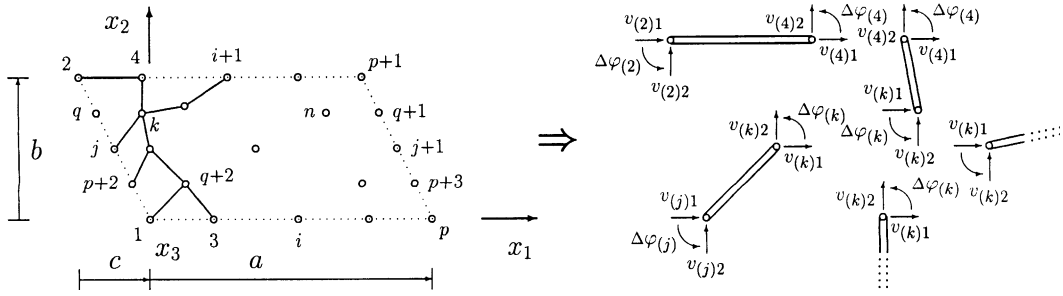

Fig. 5. Decomposition of the representative volume element.

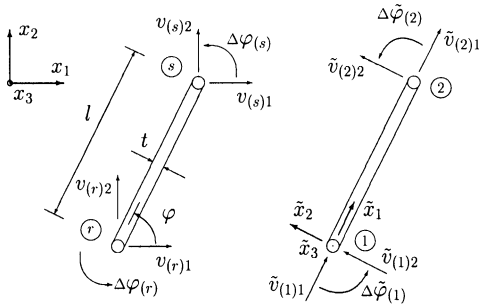

Fig. 6. Cell wall element: global and local coordinate systems.

with the node pair q and $q+1$ next to the top surface. The nodes $q+2$ to n are assigned to the internal nodes k.

3.2. Unconstrained core

A method for determination of the strain energy in the case of a cellular core which is not constrained by the face sheets has been presented by the authors in a preceding study (Hohe and Becker, 1999, 2000). Thus, only a brief outline is given here.

The deformation of the individual cell wall elements is assumed to consist of three parts, which are expressed in terms of the nodal deflections $\tilde{v}^{\mathrm{f}}_{(1)j}$, $\Delta\tilde{\varphi}_{(1)}$ and $\tilde{v}^{\mathrm{f}}_{(2)j}$, $\Delta\tilde{\varphi}_{(2)}$ of the free, unconstrained core at local nodes 1 and 2:

- homogeneously distributed longitudinal and transverse stretching on the cell wall ($\tilde{x}_1$–$\tilde{x}_3$) plane,
- bending deformation according to Euler–Bernoulli beam theory on the $\tilde{x}_1$–$\tilde{x}_2$ plane,
- homogeneously distributed transverse shear deformation on the $\tilde{x}_1$–$\tilde{x}_3$ plane.

Thus, the following cell wall displacement field is assumed:

$$\begin{aligned}
\tilde{u}^{\mathrm{f}}_1 &= \tilde{v}^{\mathrm{f}}_{(1)1} + \frac{\tilde{v}^{\mathrm{f}}_{(2)1} - \tilde{v}^{\mathrm{f}}_{(1)1}}{l}\tilde{x}_1 - \frac{1}{EI}\left(\frac{1}{2}\overline{C}_1\tilde{x}_1^2 + \overline{C}_2\tilde{x}_1 + \overline{C}_3\right)\tilde{x}_2,\\
\tilde{u}^{\mathrm{f}}_2 &= \frac{1}{EI}\left(\frac{1}{6}\overline{C}_1\tilde{x}_1^3 + \frac{1}{2}\overline{C}_2\tilde{x}_1^2 + \overline{C}_3\tilde{x}_1 + \overline{C}_4\right) - \frac{\nu}{1-\nu}\left(\frac{\tilde{v}^{\mathrm{f}}_{(2)1} - \tilde{v}^{\mathrm{f}}_{(1)1}}{l} + \overline{\varepsilon}_{33}\right)\tilde{x}_2,\\
\tilde{u}^{\mathrm{f}}_3 &= \tilde{v}^{\mathrm{f}}_{(1)3} + \frac{\tilde{v}^{\mathrm{f}}_{(2)3} - \tilde{v}^{\mathrm{f}}_{(1)3}}{l}\tilde{x}_1 + \overline{\varepsilon}_{33}\tilde{x}_3,
\end{aligned} \tag{6}$$

where E and ν are the elastic constants of the cell wall material, while h, t and l denote cell wall height, thickness and length, respectively. The constants $\overline{C}_i$ can be determined in dependence of the nodal deflections by means of the boundary conditions at the nodal points according to Euler–Bernoulli theory. The geometrical moment of inertia is denoted by I.

With the assumed displacement field (6), the strain and stress distributions in terms of the nodal deflections are easily derived by means of the linear kinematic equation and Hooke's law in consideration of the plane stress condition $\tilde{\sigma}_{22} = 0$. Subsequently, the strain energy density distribution can be evaluated. The total strain energy W^{f}_e in the cell wall element e is determined by integration of the strain energy density with respect to the volume of the cell wall element. This lengthy but straightforward calculation finally yields

$$W^{\mathrm{f}}_e = \frac{Ehtl}{2(1-\nu^2)}\left([\tilde{v}^{\mathrm{f}}_1]^{\mathrm{T}}[M_1][\tilde{v}^{\mathrm{f}}_1] + \frac{t^2}{l^2}[\tilde{v}^{\mathrm{f}}_2]^{\mathrm{T}}[M_2][\tilde{v}^{\mathrm{f}}_2] + \frac{1}{12}\frac{t^2}{l^2}[\Delta\tilde{\varphi}]^{\mathrm{T}}[M_\varphi][\Delta\tilde{\varphi}] + \frac{1-\nu}{2}[\tilde{v}^{\mathrm{f}}_3]^{\mathrm{T}}[M_3][\tilde{v}^{\mathrm{f}}_3]\right). \tag{7}$$

The generalized nodal deflection vectors $[\tilde{v}^{\mathrm{f}}_1]$, $[\tilde{v}^{\mathrm{f}}_2]$, $[\tilde{v}^{\mathrm{f}}_3]$ and $[\Delta\tilde{\varphi}]$ as well as the corresponding matrices $[M_1]$, $[M_2]$, $[M_3]$ and $[M_\varphi]$ are presented in Appendix A.1. Curved cell wall elements are approximated by polygonal cell wall elements, where the internal nodes are eliminated using the condition of force equilibrium at these nodes.

The remaining task consists in the determination of the nodal deflections. A complete linear system of equations for the nodal deflections can be derived by the following considerations:

(1) No rigid body motions of the representative volume element are permitted. Thus, without loss in generality, the following four conditions can be stated:

$$\begin{aligned} v_{(1)1} &= 0, \\ v_{(1)2} &= 0, \\ v_{(1)3} &= 0, \\ v_{(p)2} &= 0. \end{aligned} \tag{8}$$

(2) Homogeneous reference strain states $\overline{\varepsilon}_{ij}$ on the macroscopic level are considered. Therefore, all volume elements that set up the entire periodic cellular structure are deformed in the same way. Thus, periodic boundary conditions have to be applied to the representative volume element:

$$\begin{aligned} &\Delta\varphi_{(i)} = \Delta\varphi_{(i+1)}, \quad i = 1,3,\ldots,p, \\ &v_{(p)l} - v_{(i)l} = v_{(p+1)l} - v_{(i+1)l}, \quad i = 1,3,\ldots,(p-2), \;\; l = 1,2,3, \\ &\Delta\varphi_{(j)} = \Delta\varphi_{(j+1)}, \quad j = (p+2),(p+4),\ldots,q, \\ &v_{(2)l} - v_{(j)l} = v_{(p+1)l} - v_{(j+1)l}, \quad j = (p+2),(p+4),\ldots,q, \;\; l = 1,2,3, \\ &\Delta\varphi_{(1)} = \Delta\varphi_{(p)}. \end{aligned} \tag{9}$$

(3) A relation between the macroscopic reference strain state and the nodal deflections can be derived from Eq. (2). Transformation of the volume integral on the left-hand side into a surface integral by application of Green's theorem and evaluation of the integral on the right-hand side of this equation yields

$$\frac{1}{2}\frac{1}{V}\int_{\Gamma_{\mathrm{RVE}}} \left(u_i n_j + u_j n_i\right) \mathrm{d}S = \overline{\varepsilon}_{ij}, \tag{10}$$

where Γ_{RVE} is the external surface of the representative volume element, while u_i and n_i are the components of the displacement and outward normal vectors on Γ_{RVE}, respectively. If the displacements are interpolated along Γ_{RVE}, the integral in Eq. (10) can be evaluated. In consideration of the periodic boundary conditions (9), the following equations are obtained:

$$\begin{aligned} \overline{\varepsilon}_{11} &= \frac{v_{(p)1} - v_{(1)1}}{a}, \\ \overline{\varepsilon}_{22} &= \frac{v_{(2)2} - v_{(1)2}}{b} + \frac{c}{a}\frac{v_{(p)2} - v_{(1)2}}{b}, \\ \overline{\varepsilon}_{23} &= \frac{1}{2}\left(\frac{v_{(2)3} - v_{(1)3}}{b} + \frac{c}{a}\frac{v_{(p)3} - v_{(1)3}}{b}\right), \\ \overline{\varepsilon}_{13} &= \frac{1}{2}\frac{v_{(p)3} - v_{(1)3}}{a}, \\ \overline{\varepsilon}_{12} &= \frac{1}{2}\left(\frac{v_{(p)2} - v_{(1)2}}{a} + \frac{v_{(2)1} - v_{(1)1}}{b} + \frac{c}{a}\frac{v_{(p)1} - v_{(1)1}}{b}\right). \end{aligned} \tag{11}$$

(4) Since no external forces are acting, the forces and moments at all internal nodes as well as on all pairs of corresponding nodes on Γ_{RVE} have to satisfy the equilibrium conditions:

$$\left.\begin{aligned} F_{(1)l} + F_{(2)l} + F_{(p)l} + F_{(p+1)l} &= 0, \\ M_{(1)} + M_{(2)} + M_{(p)} + M_{(p+1)} &= 0, \\ \left.\begin{aligned} F_{(i)l} + F_{(i+1)l} &= 0 \\ M_{(i)} + M_{(i+1)} &= 0 \end{aligned}\right\}, &\quad \begin{cases} i = 3,5,\ldots,(p-2) \\ i = (p+2),(p+4),\ldots,q \end{cases} \\ \left.\begin{aligned} F_{(k)l} &= 0 \\ M_{(k)} &= 0 \end{aligned}\right\}, &\quad k = (q+2),(q+3),\ldots n. \end{aligned}\right\} l = 1,2,3. \tag{12}$$

The nodal forces $F_{(i)j}$ and moments $M_{(i)}$ can be determined in terms of the nodal deflections by partial differentiation of Eq. (7) with respect to the nodal deflections. It should be noted that the global equilibrium with respect to the forces is satisfied identically, since the local displacement field assumed for the cell wall elements is derived in consideration of the local equilibrium conditions. Therefore, three of the Eq. (12) are already satisfied identically and thus have to be omitted. The system (8)–(12) is easily solved by Gaussian elimination.

3.3. Perfectly constrained core

In general, the displacement field (6) assumed in Section 3.2 is incompatible with the mode of deformation of the face sheets. A displacement field which is compatible with the deformation of the face sheets can be obtained by the extension of the displacement field of the face sheets into the core region. If rigid body motions are suppressed by stating boundary conditions similar to Eq. (8), the displacements of the nodal points in the case of a perfectly constrained core are given by

$$\begin{aligned} v^{c}_{(i)1} &= x_{(i)1}\overline{\varepsilon}_{11} + 2x_{(i)2}\overline{\varepsilon}_{12}, \\ v^{c}_{(i)2} &= x_{(i)2}\overline{\varepsilon}_{22}, \\ v^{c}_{(i)3} &= 2x_{(i)1}\overline{\varepsilon}_{13} + 2x_{(i)2}\overline{\varepsilon}_{23}, \end{aligned} \tag{13}$$

where $x_{(i)j}$ denotes the coordinate x_j of nodal point i. Again, macroscopically homogeneous reference strain states $\overline{\varepsilon}_{ij}$ are considered.

A displacement field for the mid-plane of an individual cell wall element which is compatible with the mode of deformation of the face sheets is obtained by a linear interpolation between the nodal points. In consideration of the local plane stress condition $\tilde{\sigma}_{22} = 0$, the displacement field of the cell wall element with respect to the local system $\tilde{x}_i$ is given by

$$\begin{aligned} \tilde{u}^{c}_{1} &= \tilde{v}^{c}_{(1)1} + \frac{\tilde{v}^{c}_{(2)1} - \tilde{v}^{c}_{(1)1}}{l}\tilde{x}_1, \\ \tilde{u}^{c}_{2} &= \tilde{v}^{c}_{(1)2} + \frac{\tilde{v}^{c}_{(2)2} - \tilde{v}^{c}_{(1)2}}{l}\tilde{x}_1 - \frac{\nu}{1-\nu}\left(\frac{\tilde{v}^{c}_{(2)1} - \tilde{v}^{c}_{(1)1}}{l} + \overline{\varepsilon}_{33}\right)\tilde{x}_2, \\ \tilde{u}^{c}_{3} &= \tilde{v}^{c}_{(1)3} + \frac{\tilde{v}^{c}_{(2)3} - \tilde{v}^{c}_{(1)3}}{l}\tilde{x}_1 + \overline{\varepsilon}_{33}\tilde{x}_3. \end{aligned} \tag{14}$$

The strain energy W^{c}_{e} in the cell wall element associated with the displacement field (14) can be determined in a way analogous to the case of the unconstrained core (Section 3.2). The following result is obtained:

$$W^{c}_{e} = \frac{Ehtl}{2(1-\nu^2)}\left([\tilde{v}^{c}_{1}]^{T}[M_1][\tilde{v}^{c}_{1}] + \frac{1-\nu}{2}[\tilde{v}^{c}_{3}]^{T}[M_3][\tilde{v}^{c}_{3}]\right). \tag{15}$$

The generalized nodal deflection vectors $[\tilde{v}^{c}_{i}]$ are presented in Appendix A.2. Since kinematically admissible displacement and strain fields have been assumed, the normal and shear components $\overline{C}^{c}_{1111}$, $\overline{C}^{c}_{2222}$, $\overline{C}^{c}_{3333}$, $\overline{C}^{c}_{2323}$, $\overline{C}^{c}_{1313}$ and $\overline{C}^{c}_{1212}$ obtained from Eq. (15) in conjunction with Eq. (5) define Voigt type bounds (Voigt, 1889; Hill, 1952) for the actual normal and shear properties of the cellular core.

3.4. Superposition

3.4.1. Shear formulation

A method for derivation of an improved assumed displacement field has been proposed by Becker (1998). The basic idea of this approach is the assumption that the total displacement field of the cellular

core can be described by a weighted superposition of the displacement fields associated with the unconstrained and the perfectly constrained core. Within this concept, the weight function has to be chosen in such a way that at the face sheets, the displacement field of the perfectly constrained core is obtained, while far from the face sheets in an infinitely thick core, the displacement field of the unconstrained core is approached.

In the original study, the method is restricted to regular hexagonal cores with thin cell walls. A generalization to the element based approach of the present study yields the following displacement field on cell wall element level:

$$\begin{aligned}
\tilde{u}_1(\tilde{x}_i) &= \tilde{u}_1^{\mathrm{c}}(\tilde{x}_i) f(\tilde{x}_3) + \tilde{u}_1^{\mathrm{f}}(\tilde{x}_i)(1 - f(\tilde{x}_3)) + \Delta\tilde{u}_1 f(\tilde{x}_3), \\
\tilde{u}_2(\tilde{x}_i) &= \tilde{u}_2^{\mathrm{c}}(\tilde{x}_i) f(\tilde{x}_3) + \tilde{u}_2^{\mathrm{f}}(\tilde{x}_i)(1 - f(\tilde{x}_3)) + \Delta\tilde{u}_2 f(\tilde{x}_3), \\
\tilde{u}_3(\tilde{x}_i) &= \tilde{u}_3^{\mathrm{c}}(\tilde{x}_i) f(\tilde{x}_3) + \tilde{u}_3^{\mathrm{f}}(\tilde{x}_i)(1 - f(\tilde{x}_3)) + \Delta\tilde{u}_3 f(\tilde{x}_3).
\end{aligned} \tag{16}$$

In Eq. (16), the displacement field $\tilde{u}_i^{\mathrm{c}}$ of the perfectly constrained core and $\tilde{u}_i^{\mathrm{f}}$ of the free, unconstrained core are given in terms of the nodal deflections as described in Sections 3.2 and 3.3, respectively. The global function

$$f = \frac{\cosh\left(\lambda \frac{2\tilde{x}_3}{h}\right)}{\cosh(\lambda)} = \frac{\cosh\left(\lambda \frac{2x_3}{h}\right)}{\cosh(\lambda)} \tag{17}$$

describes the decay from the displacement field of the face sheets to the displacement field associated with the unconstrained core. The decay rate is controlled by the global parameter λ. The parameters $\Delta\tilde{u}_1$, $\Delta\tilde{u}_2$ and $\Delta\tilde{u}_3$ follow from the transformation of the global parameters Δu_1, Δu_2 and Δu_3, which describe the relative lateral displacement of the coordinate systems for description of $\tilde{u}_1^{\mathrm{c}}$ and $\tilde{u}_1^{\mathrm{f}}$. This relative displacement has to be considered, since coordinate systems which are fixed to the body have been used in both cases (Eqs. (8) and (13), respectively).

Alternative decay functions might be used instead of Eq. (17). Nevertheless, the mathematical description of decay processes usually results in exponential functions of the distance. Thus, a function of the type $\cosh x_3$ as in Eq. (17) might be an appropriate choice.

The strain energy W_e^{s} associated to the displacement field (16) is evaluated analogous to the cases of the unconstrained and the perfectly constrained core. The result reads

$$W_e^{\mathrm{s}} = \frac{Ehtl}{2(1-\nu^2)} \left(\hat{w}^{\mathrm{cc}} f^{\mathrm{cc}} + \hat{w}^{\mathrm{cf}} f^{\mathrm{cf}} + \hat{w}^{\mathrm{ff}} f^{\mathrm{ff}} + \hat{w}^{\mathrm{aa}} f^{\mathrm{aa}}\right) \tag{18}$$

with

$$\begin{aligned}
f^{\mathrm{cc}} &= \frac{2\lambda + \sinh(2\lambda)}{4\lambda \cosh^2(\lambda)}, \\
f^{\mathrm{cf}} &= 2\frac{-2\lambda + \sinh(2\lambda)}{4\lambda \cosh^2(\lambda)}, \\
f^{\mathrm{ff}} &= \frac{4\lambda + 2\lambda\cosh(2\lambda) - 3\sinh(2\lambda)}{4\lambda \cosh^2(\lambda)}, \\
f^{\mathrm{aa}} &= \frac{-2\lambda^2 + \lambda \sinh(2\lambda)}{\cosh^2(\lambda)}.
\end{aligned} \tag{19}$$

The dimensionless strain energy components are given by

$$
\begin{aligned}
\hat{w}^{\mathrm{cc}} &= [\tilde{v}_1^{\mathrm{c}}]^{\mathrm{T}}[M_1][\tilde{v}_1^{\mathrm{c}}] + \frac{1-\nu}{2}[\tilde{v}_3^{\mathrm{c}}]^{\mathrm{T}}[M_3][\tilde{v}_3^{\mathrm{c}}],\\
\hat{w}^{\mathrm{cf}} &= [\tilde{v}_1^{\mathrm{c}}]^{\mathrm{T}}[M_1][\tilde{v}_1^{\mathrm{f}}] + \frac{1-\nu}{2}[\tilde{v}_3^{\mathrm{c}}]^{\mathrm{T}}[M_3][\tilde{v}_3^{\mathrm{f}}],\\
\hat{w}^{\mathrm{ff}} &= [\tilde{v}_1^{\mathrm{f}}]^{\mathrm{T}}[M_1][\tilde{v}_1^{\mathrm{f}}] + \frac{t^2}{l^2}[\tilde{v}_2^{\mathrm{f}}]^{\mathrm{T}}[M_2][\tilde{v}_2^{\mathrm{f}}] + \frac{1}{12}\frac{t^2}{l^2}[\Delta\tilde{\varphi}]^{\mathrm{T}}[M_\varphi][\Delta\tilde{\varphi}] + \frac{1-\nu}{2}[\tilde{v}_3^{\mathrm{f}}]^{\mathrm{T}}[M_3][\tilde{v}_3^{\mathrm{f}}],\\
\hat{w}^{\mathrm{aa}} &= \frac{1-\nu}{6}\frac{l^2}{h^2}[\tilde{v}_1^{\mathrm{a}}]^{\mathrm{T}}[M_{\mathrm{a}}][\tilde{v}_1^{\mathrm{a}}] + \frac{1}{24}\frac{\nu^2}{1-\nu}\frac{t^2}{h^2}\left([\tilde{v}_1^{\mathrm{c}*}]^{\mathrm{T}}[M_1][\tilde{v}_1^{\mathrm{c}*}] - 2[\tilde{v}_1^{\mathrm{c}*}]^{\mathrm{T}}[M_1][\tilde{v}_1^{\mathrm{f}*}] + [\tilde{v}_1^{\mathrm{f}*}]^{\mathrm{T}}[M_1][\tilde{v}_1^{\mathrm{f}*}]\right)\\
&\quad + \frac{1-\nu}{6}\frac{l^2}{h^2}[\tilde{v}_2^{\mathrm{a}}]^{\mathrm{T}}[M_{\mathrm{a}}][\tilde{v}_2^{\mathrm{a}}] + \frac{1-\nu}{24}\frac{t^2}{h^2}[\tilde{v}_2^{\mathrm{c}}]^{\mathrm{T}}[M_2][\tilde{v}_2^{\mathrm{c}}] - \frac{1-\nu}{60}\frac{l^2}{h^2}[\tilde{v}_2^{\mathrm{c}}]^{\mathrm{T}}[M_2][\tilde{v}_2^{\mathrm{f}}]\\
&\quad + \frac{1-\nu}{40}\left(\frac{3}{7}+\frac{1}{3}\frac{t^2}{l^2}\right)\frac{l^2}{h^2}[\tilde{v}_2^{\mathrm{f}}]^{\mathrm{T}}[M_2][\tilde{v}_2^{\mathrm{f}}] - \frac{1-\nu}{12}\frac{t^2}{h^2}[\tilde{v}_2^{\mathrm{c}}]^{\mathrm{T}}[M_2^*][\tilde{v}_2^{\mathrm{f}}] + \frac{1-\nu}{120}\left(1+5\frac{t^2}{l^2}\right)\frac{l^2}{h^2}[\tilde{v}_2^{\mathrm{f}}]^{\mathrm{T}}[M_2^*][\tilde{v}_2^{\mathrm{f}}]\\
&\quad + \frac{1-\nu}{72}\frac{t^2}{h^2}[\Delta\tilde{\varphi}]^{\mathrm{T}}[M_\varphi^*][\Delta\tilde{\varphi}] + \frac{1}{3}\frac{l^2}{h^2}[\tilde{v}_3^{\mathrm{a}}]^{\mathrm{T}}[M_{\mathrm{a}}][\tilde{v}_3^{\mathrm{a}}].
\end{aligned}
\tag{20}
$$

The generalized nodal deflection vectors and the corresponding matrices are given in Appendices A.1–A.3. Note that the first term in Eq. (18) is the weighted strain energy for the perfectly constrained core, while the third term is the weighted strain energy associated with the unconstrained core.

In Eqs. (18)–(20), the nodal deflections for the unconstrained and the perfectly constrained core are determined according to Sections 3.2 and 3.3. The global parameters λ and Δu_i are determined by application of the principle of minimum strain energy. The minimization of the total strain energy in the entire representative volume element is performed by a numerical two step scheme. In the first step, a rough estimate for λ and Δu_i is determined by the method of nested intervals. In the second step, a high accuracy solution of the problem

$$
\begin{aligned}
&\frac{\partial W_{\mathrm{tot}}^{\mathrm{s}}}{\partial\lambda} = 0,\\
&\frac{\partial W_{\mathrm{tot}}^{\mathrm{s}}}{\partial\Delta u_i} = 0, \quad i = 1,2,3,\\
&\quad \text{where } W_{\mathrm{tot}}^{\mathrm{s}} = \sum_e W_e^{\mathrm{s}}
\end{aligned}
\tag{21}
$$

is determined by means of Newton's method using the solution of the first step as the starting point.

The displacement field (16) is determined by a direct superposition of the displacement field in case of the unconstrained core and the displacement field of the perfectly constrained core. In both cases, it is assumed that plane cross-sections of the cell wall elements which have initially been parallel to the global sandwich plane (global x_1–x_2 plane) remain plane and parallel to the global x_1–x_2 plane. Hence, it is implied that these cross-sections remain plane and parallel to the global x_1–x_2 plane even if the total displacement field (16) is considered. Thus, this formulation does not account for cell wall bending with respect to the local $\tilde{x}_1$-axis which can occur in the transition zone next to the face sheets (Fig. 2). Within this formulation, the transition from the displacement field of the face sheets to the deformation of the unconstrained core is associated with pure shear deformation in the $\tilde{x}_2$–$\tilde{x}_3$ plane. Therefore, this formulation is subsequently termed "shear formulation".

3.4.2. Bending formulation

As mentioned earlier, the assumption for the displacement field made in Section 3.4.1 does not account for bending with respect to the longitudinal axes in the transition zone. Therefore, especially for thick cell

walls, this formulation overestimates the strain energy. In order to account for these bending effects, the displacement field (16) is modified by adding an additional displacement in $\tilde{x}_3$-direction which is governed by the slope $\partial\tilde{u}_2/\partial\tilde{x}_3$ of the cell wall in $\tilde{x}_3$-direction. Thus, Eq. (16) is replaced by

$$\begin{aligned}
\tilde{u}_1(\tilde{x}_i) &= \tilde{u}_1^{\mathrm{c}}(\tilde{x}_i)f(\tilde{x}_3) + \tilde{u}_1^{\mathrm{f}}(\tilde{x}_i)(1-f(\tilde{x}_3)) + \Delta\tilde{u}_1 f(\tilde{x}_3),\\
\tilde{u}_2(\tilde{x}_i) &= \tilde{u}_2^{\mathrm{c}}(\tilde{x}_i)f(\tilde{x}_3) + \tilde{u}_2^{\mathrm{f}}(\tilde{x}_i)(1-f(\tilde{x}_3)) + \Delta\tilde{u}_2 f(\tilde{x}_3),\\
\tilde{u}_3(\tilde{x}_i) &= \tilde{u}_3^{\mathrm{c}}(\tilde{x}_i)f(\tilde{x}_3) + \tilde{u}_3^{\mathrm{f}}(\tilde{x}_i)(1-f(\tilde{x}_3)) + \Delta\tilde{u}_3 f(\tilde{x}_3) - \tilde{x}_2\left.\frac{\partial\tilde{u}_2}{\partial\tilde{x}_3}\right|_{\tilde{x}_2=0}.
\end{aligned} \tag{22}$$

The strain energy W_e^{b} associated with the displacement field (22) is given by

$$W_e^{\mathrm{b}} = \frac{Ehtl}{2(1-\nu^2)}\left(\hat{w}^{\mathrm{cc}}f^{\mathrm{cc}} + \hat{w}^{\mathrm{cf}}f^{\mathrm{cf}} + \hat{w}^{\mathrm{ff}}f^{\mathrm{ff}} + \hat{w}^{\mathrm{fb}}f^{\mathrm{fb}} + \hat{w}^{\mathrm{aa}}f^{\mathrm{aa}} + \hat{w}^{\mathrm{bb}}f^{\mathrm{bb}}\right) \tag{23}$$

with

$$\begin{aligned}
f^{\mathrm{cc}} &= \frac{2\lambda + \sinh(2\lambda)}{4\lambda\cosh^2(\lambda)},\\
f^{\mathrm{cf}} &= 2\frac{-2\lambda + \sinh(2\lambda)}{4\lambda\cosh^2(\lambda)},\\
f^{\mathrm{ff}} &= \frac{4\lambda + 2\lambda\cosh(2\lambda) - 3\sinh(2\lambda)}{4\lambda\cosh^2(\lambda)},\\
f^{\mathrm{fb}} &= 2\frac{-2\lambda^2 + \lambda\sinh(2\lambda)}{\cosh^2(\lambda)},\\
f^{\mathrm{aa}} &= \frac{-2\lambda^2 + \lambda\sinh(2\lambda)}{\cosh^2(\lambda)},\\
f^{\mathrm{bb}} &= \frac{2\lambda^4 + \lambda^3\sinh(2\lambda)}{\cosh^2(\lambda)},
\end{aligned} \tag{24}$$

where the dimensionless strain energy components are given by

$$\begin{aligned}
\hat{w}^{\mathrm{cc}} &= [\tilde{v}_1^{\mathrm{c}}]^{\mathrm{T}}[M_1][\tilde{v}_1^{\mathrm{c}}] + \frac{1-\nu}{2}[\tilde{v}_3^{\mathrm{c}}]^{\mathrm{T}}[M_3][\tilde{v}_3^{\mathrm{c}}],\\
\hat{w}^{\mathrm{cf}} &= [\tilde{v}_1^{\mathrm{c}}]^{\mathrm{T}}[M_1][\tilde{v}_1^{\mathrm{f}}] + \frac{1-\nu}{2}[\tilde{v}_3^{\mathrm{c}}]^{\mathrm{T}}[M_3][\tilde{v}_3^{\mathrm{f}}],\\
\hat{w}^{\mathrm{ff}} &= [\tilde{v}_1^{\mathrm{f}}]^{\mathrm{T}}[M_1][\tilde{v}_1^{\mathrm{f}}] + \frac{t^2}{l^2}[\tilde{v}_2^{\mathrm{f}}]^{\mathrm{T}}[M_2][\tilde{v}_2^{\mathrm{f}}] + \frac{1}{12}\frac{t^2}{l^2}[\Delta\tilde{\varphi}]^{\mathrm{T}}[M_\varphi][\Delta\tilde{\varphi}] + \frac{1-\nu}{2}[\tilde{v}_3^{\mathrm{f}}]^{\mathrm{T}}[M_3][\tilde{v}_3^{\mathrm{f}}],\\
\hat{w}^{\mathrm{fb}} &= -\frac{\nu}{12}\frac{t^2}{h^2}[\tilde{v}_2^{\mathrm{c}}]^{\mathrm{T}}[M_2][\tilde{v}_2^{\mathrm{f}}] + \frac{7\nu}{120}\frac{t^2}{h^2}[\tilde{v}_2^{\mathrm{f}}]^{\mathrm{T}}[M_2][\tilde{v}_2^{\mathrm{f}}] + \frac{\nu}{24}\frac{t^2}{h^2}[\tilde{v}_2^{\mathrm{f}}]^{\mathrm{T}}[M_2^*][\tilde{v}_2^{\mathrm{f}}] - \frac{\nu}{720}\frac{t^2}{h^2}[\Delta\tilde{\varphi}]^{\mathrm{T}}[M_\varphi][\Delta\tilde{\varphi}]\\
&\quad + \frac{\nu}{3}\frac{t^2}{h^2}[\Delta\tilde{\varphi}^{\mathrm{a}}]^{\mathrm{T}}[M_{\mathrm{a}}][\tilde{v}_2^{\mathrm{a}}],
\end{aligned}$$

$$\begin{aligned}
\hat{w}^{\mathrm{aa}} &= \frac{1-\nu}{6}\frac{l^2}{h^2}[\tilde{v}_1^{\mathrm{a}}]^{\mathrm{T}}[M_{\mathrm{a}}][\tilde{v}_1^{\mathrm{a}}] + \frac{1}{24}\frac{\nu^2}{1-\nu}\frac{t^2}{h^2}\left([\tilde{v}_1^{\mathrm{c}*}]^{\mathrm{T}}[M_1][\tilde{v}_1^{\mathrm{c}*}] - 2[\tilde{v}_1^{\mathrm{c}*}]^{\mathrm{T}}[M_1][\tilde{v}_1^{\mathrm{f}*}] + [\tilde{v}_1^{\mathrm{f}*}]^{\mathrm{T}}[M_1][\tilde{v}_1^{\mathrm{f}*}]\right) \\
&\quad + \frac{1-\nu}{6}\frac{t^2}{h^2}[\tilde{v}_2^{\mathrm{a}}]^{\mathrm{T}}[M_{\mathrm{a}}][\tilde{v}_2^{\mathrm{a}}] + \frac{1-\nu}{30}\frac{t^2}{h^2}[\tilde{v}_2^{\mathrm{f}}]^{\mathrm{T}}[M_2][\tilde{v}_2^{\mathrm{f}}] - \frac{1-\nu}{3}\frac{t^2}{h^2}[\tilde{v}_2^{\mathrm{c}}]^{\mathrm{T}}[M_2^*][\tilde{v}_2^{\mathrm{f}}] + \frac{1-\nu}{6}\frac{t^2}{h^2}[\tilde{v}_2^{\mathrm{f}}]^{\mathrm{T}}[M_2^*][\tilde{v}_2^{\mathrm{f}}] \\
&\quad + \frac{1-\nu}{18}\frac{t^2}{h^2}[\Delta\tilde{\varphi}]^{\mathrm{T}}[M_\varphi^*][\Delta\tilde{\varphi}] + \frac{1}{3}\frac{l^2}{h^2}[\tilde{v}_3^{\mathrm{a}}]^{\mathrm{T}}[M_{\mathrm{a}}][\tilde{v}_3^{\mathrm{a}}], \\
\hat{w}^{\mathrm{bb}} &= \frac{1}{9}\frac{t^2l^2}{h^4}[\tilde{v}_2^{\mathrm{a}}]^{\mathrm{T}}[M_{\mathrm{a}}][\tilde{v}_2^{\mathrm{a}}] - \frac{1}{90}\frac{t^2l^2}{h^4}[\tilde{v}_2^{\mathrm{c}}]^{\mathrm{T}}[M_2][\tilde{v}_2^{\mathrm{f}}] + \frac{1}{140}\frac{t^2l^2}{h^4}[\tilde{v}_2^{\mathrm{f}}]^{\mathrm{T}}[M_2][\tilde{v}_2^{\mathrm{f}}] + \frac{1}{180}\frac{t^2l^2}{h^4}[\tilde{v}_2^{\mathrm{f}}]^{\mathrm{T}}[M_2^*][\tilde{v}_2^{\mathrm{f}}].
\end{aligned} \tag{25}$$

The generalized nodal deflection vectors and the associated matrices are given in Appendices A.1–A.3. Note that in comparison to the shear formulation (18)–(20), the integrated weight functions f^{cc}, f^{cf}, f^{ff} and f^{aa} as well as the dimensionless energy components $\hat{w}^{\mathrm{cc}}$, $\hat{w}^{\mathrm{cf}}$ and $\hat{w}^{\mathrm{ff}}$ remain unchanged while a different result is obtained in case of $\hat{w}^{\mathrm{aa}}$.

3.4.3. Reduced integration

The formulation (23)–(25) accounts for the bending effects which are neglected in the shear formulation. Nevertheless, both formulations for the displacement field of a single cell wall yield rather lengthy and complicated results for the strain energy. Since most of the terms in the expression for $\hat{w}^{\mathrm{fb}}$, $\hat{w}^{\mathrm{aa}}$ and $\hat{w}^{\mathrm{bb}}$ depend on t^2/h^2 (Eq. (25)), these terms are small compared to most terms in the expressions for $\hat{w}^{\mathrm{cc}}$, $\hat{w}^{\mathrm{cf}}$ and $\hat{w}^{\mathrm{ff}}$ in the limit $t \ll h$ of thin cell walls and reasonable core thickness.

A simplified expression for the strain energy in consideration of bending with respect to the longitudinal axis in the transition zone can be derived by the application of a "reduced integration" scheme to the integration of the strain energy density with respect to the cell wall volume. Hence the cell wall thickness t in most cases is small compared to the other cell wall dimensions ($t \ll l, h$), the integral with respect to the cell wall thickness ($\tilde{x}_2$-) direction is replaced by the product of the integrand on the mid-plane of the cell wall and the cell wall thickness. This method can be interpreted as a replacement of the real distribution of the strain energy density in $\tilde{x}_2$-direction by a linear distribution. The linear function is integrated numerically by means of a one point Gauss integration scheme which yields the exact result in case of linear integrands.

Application of the reduced integration scheme to the strain energy distribution associated with the assumed displacement field (22) for the individual cell wall elements yields

$$W_e^{\mathrm{ri}} = \frac{Ehtl}{2(1-\nu^2)}(\hat{w}^{\mathrm{cc}}f^{\mathrm{cc}} + \hat{w}^{\mathrm{cf}}f^{\mathrm{cf}} + \hat{w}^{\mathrm{ff}}f^{\mathrm{ff}} + \hat{w}^{\mathrm{aa}}f^{\mathrm{aa}}), \tag{26}$$

where

$$\begin{aligned}
f^{\mathrm{cc}} &= \frac{2\lambda + \sinh(2\lambda)}{4\lambda\cosh^2(\lambda)}, \\
f^{\mathrm{cf}} &= 2\frac{-2\lambda + \sinh(2\lambda)}{4\lambda\cosh^2(\lambda)}, \\
f^{\mathrm{ff}} &= \frac{4\lambda + 2\lambda\cosh(2\lambda) - 3\sinh(2\lambda)}{4\lambda\cosh^2(\lambda)}, \\
f^{\mathrm{aa}} &= \frac{-2\lambda^2 + \lambda\sinh(2\lambda)}{\cosh^2(\lambda)},
\end{aligned} \tag{27}$$

and

$$
\begin{aligned}
\hat{w}^{\mathrm{cc}} &= [\tilde{v}_1^{\mathrm{c}}]^{\mathrm{T}}[M_1][\tilde{v}_1^{\mathrm{c}}] + \frac{1-\nu}{2}[\tilde{v}_3^{\mathrm{c}}]^{\mathrm{T}}[M_3][\tilde{v}_3^{\mathrm{c}}],\\
\hat{w}^{\mathrm{cf}} &= [\tilde{v}_1^{\mathrm{c}}]^{\mathrm{T}}[M_1][\tilde{v}_1^{\mathrm{f}}] + \frac{1-\nu}{2}[\tilde{v}_3^{\mathrm{c}}]^{\mathrm{T}}[M_3][\tilde{v}_3^{\mathrm{f}}],\\
\hat{w}^{\mathrm{ff}} &= [\tilde{v}_1^{\mathrm{f}}]^{\mathrm{T}}[M_1][\tilde{v}_1^{\mathrm{f}}] + \frac{1-\nu}{2}[\tilde{v}_3^{\mathrm{f}}]^{\mathrm{T}}[M_3][\tilde{v}_3^{\mathrm{f}}],\\
\hat{w}^{\mathrm{aa}} &= \frac{1-\nu}{6}\frac{l^2}{h^2}[\tilde{v}_1^{\mathrm{a}}]^{\mathrm{T}}[M_{\mathrm{a}}][\tilde{v}_1^{\mathrm{a}}] + \frac{1}{3}\frac{l^2}{h^2}[\tilde{v}_3^{\mathrm{a}}]^{\mathrm{T}}[M_{\mathrm{a}}][\tilde{v}_3^{\mathrm{a}}].
\end{aligned}
\tag{28}
$$

Note that the expressions (27) for f^{cc}, f^{cf}, f^{ff} and f^{aa} are identical to the corresponding expressions (19) in case of the shear formulation.

Obviously, expressions (26)–(28) for the strain energy W_e^{ri} in case of the reduced integration scheme are much more simple than the corresponding expressions (23)–(25) for the strain energy W_e^{b} in case of the full integration scheme. Nevertheless, due to the omission of the terms corresponding to the displacement in $\tilde{x}_2$-direction in the expression for $\hat{w}^{\mathrm{ff}}$ in Eq. (28) (Eq. (25) or Eq. (20) for comparison), the formulation (26)–(28) fails to approach the limit of the free, unconstrained core if $h \to \infty$ and thus $\lambda \to \infty$.

A pragmatic way to avoid this problem consists in application of a "selective reduced integration" scheme, where the reduced integration scheme is applied only to the additional terms $\hat{w}^{\mathrm{cf}}$, $\hat{w}^{\mathrm{fb}}$, $\hat{w}^{\mathrm{aa}}$ and $\hat{w}^{\mathrm{bb}}$, while the full analytic integration scheme is applied to the components $\hat{w}^{\mathrm{cc}}$ and $\hat{w}^{\mathrm{ff}}$ which represent the limit cases of the perfectly constrained core and the unconstrained core, respectively. Application of the selective reduced integration scheme to the assumed displacement field (22) yields

$$
W_e^{\mathrm{si}} = \frac{Ehtl}{2(1-\nu^2)}(\hat{w}^{\mathrm{cc}} f^{\mathrm{cc}} + \hat{w}^{\mathrm{cf}} f^{\mathrm{cf}} + \hat{w}^{\mathrm{ff}} f^{\mathrm{ff}} + \hat{w}^{\mathrm{aa}} f^{\mathrm{aa}}),
\tag{29}
$$

where again

$$
\begin{aligned}
f^{\mathrm{cc}} &= \frac{2\lambda + \sinh(2\lambda)}{4\lambda\cosh^2(\lambda)},\\
f^{\mathrm{cf}} &= 2\frac{-2\lambda + \sinh(2\lambda)}{4\lambda\cosh^2(\lambda)},\\
f^{\mathrm{ff}} &= \frac{4\lambda + 2\lambda\cosh(2\lambda) - 3\sinh(2\lambda)}{4\lambda\cosh^2(\lambda)},\\
f^{\mathrm{aa}} &= \frac{-2\lambda^2 + \lambda\sinh(2\lambda)}{\cosh^2(\lambda)},
\end{aligned}
\tag{30}
$$

and

$$
\begin{aligned}
\hat{w}^{\mathrm{cc}} &= [\tilde{v}_1^{\mathrm{c}}]^{\mathrm{T}}[M_1][\tilde{v}_1^{\mathrm{c}}] + \frac{1-\nu}{2}[\tilde{v}_3^{\mathrm{c}}]^{\mathrm{T}}[M_3][\tilde{v}_3^{\mathrm{c}}],\\
\hat{w}^{\mathrm{cf}} &= [\tilde{v}_1^{\mathrm{c}}]^{\mathrm{T}}[M_1][\tilde{v}_1^{\mathrm{f}}] + \frac{1-\nu}{2}[\tilde{v}_3^{\mathrm{c}}]^{\mathrm{T}}[M_3][\tilde{v}_3^{\mathrm{f}}],\\
\hat{w}^{\mathrm{ff}} &= [\tilde{v}_1^{\mathrm{f}}]^{\mathrm{T}}[M_1][\tilde{v}_1^{\mathrm{f}}] + \frac{t^2}{l^2}[\tilde{v}_2^{\mathrm{f}}]^{\mathrm{T}}[M_2][\tilde{v}_2^{\mathrm{f}}] + \frac{1}{12}\frac{t^2}{l^2}[\Delta\tilde{\varphi}]^{\mathrm{T}}[M_\varphi][\Delta\tilde{\varphi}] + \frac{1-\nu}{2}[\tilde{v}_3^{\mathrm{f}}]^{\mathrm{T}}[M_3][\tilde{v}_3^{\mathrm{f}}],\\
\hat{w}^{\mathrm{aa}} &= \frac{1-\nu}{6}\frac{l^2}{h^2}[\tilde{v}_1^{\mathrm{a}}]^{\mathrm{T}}[M_{\mathrm{a}}][\tilde{v}_1^{\mathrm{a}}] + \frac{1}{3}\frac{l^2}{h^2}[\tilde{v}_3^{\mathrm{a}}]^{\mathrm{T}}[M_{\mathrm{a}}][\tilde{v}_3^{\mathrm{a}}].
\end{aligned}
\tag{31}
$$

With Eqs. (29)–(31), a sufficiently simple expression for the strain energy in a single cell wall is obtained, which accounts for bending with respect to the longitudinal axis in the transition zone and approaches both the limit of the perfectly constrained core for $h \to 0$ and the limit of the unconstrained core for $h \to \infty$.

The expressions (26)–(28) for the reduced integration scheme can also be derived from the expressions (23)–(25) for the strain energy W_e^{b} by neglect of all terms in Eq. (25), which are proportional either to t^2/l^2 or t^2/h^2. The expressions (29)–(31) for the selective reduced integration scheme can be derived from the corresponding expressions in case of the bending formulation if only the terms which are proportional to t^2/h^2 are neglected in Eq. (25). Note that both the shear and the bending formulation in conjunction with full analytical integration are based on kinematically admissible displacement and strain fields in conjunction with the principle of minimum strain energy and therefore define rigorous Voigt type bounds for the effective moduli. The formulations based on the reduced and the selective reduced integration schemes do not define rigorous bounds for the effective properties since terms in the energy expressions have been omitted.

4. Numerical reference solution

A reference solution for the analytical approaches is determined by means of the finite element method. Thus, the cell walls are meshed by displacement based four node shell elements. A shear flexible theory in an enhanced strain formulation with full integration is employed to avoid spurious modes of deformation as well as locking effects which might occur in the case of very short cell walls. A finite element formulation with six degrees of freedom per node is used.

The finite element model is loaded by prescribed displacements at the top and bottom surface according to the displacement field of the face sheets. Thus, the following displacements are imposed to the nodes at $x_3 = \pm h/2$:

$$u_i^0 = \begin{pmatrix} x_1\overline{\varepsilon}_{11} + 2x_2\overline{\varepsilon}_{12} + 2x_3\overline{\varepsilon}_{13} \\ x_2\overline{\varepsilon}_{22} + 2x_3\overline{\varepsilon}_{23} \\ x_3\overline{\varepsilon}_{33} \end{pmatrix}. \tag{32}$$

Periodic boundary conditions are applied to the other external surfaces of the representative volume element. Thus,

$$\left.\begin{array}{l} v_{(i)l}(x_3) - v_{(i)l}\left(\frac{h}{2}\right) = v_{(i+1)l}(x_3) - v_{(i+1)l}\left(\frac{h}{2}\right), \\ \Delta\varphi_{(i)l}(x_3) = \Delta\varphi_{(i+1)l}(x_3), \end{array}\right\}, \quad \left\{\begin{array}{l} i = 1,3,\ldots,q \\ l = 1,2,3, \end{array}\right. \tag{33}$$

where $v_{(i)l}(x_3)$ denotes the displacement of a finite element node on cell wall intersection i at x_3 with respect to direction x_l, while $\Delta\varphi_{(i)l}(x_3)$ denotes the rotation of a finite element node on cell wall intersection i at x_3 with respect to the x_l-axis.

As in case of the analytical determination of the strain energy, all 21 reference strain states, where a maximum of two components of the macroscopic strain tensor $\overline{\varepsilon}_{ij}$ have non-zero values, are applied to the representative volume element. For all strain states the total strain energy is computed. Subsequently, the components $\overline{C}_{ijkl}$ of the effective elasticity tensor are evaluated by means of Eq. (5).

5. Examples

The analytical methods derived in Section 3 are applied to three example core geometries (Fig. 7). First a low-density hexagonal core is considered. A moderate-density tubular core is analyzed as the second

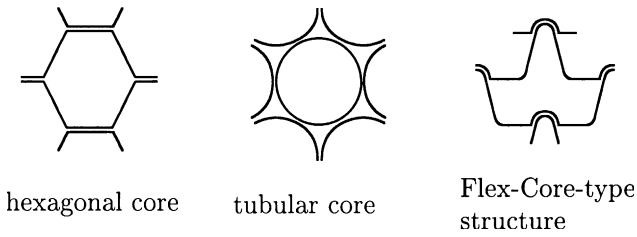

Fig. 7. Example sandwich core geometries.

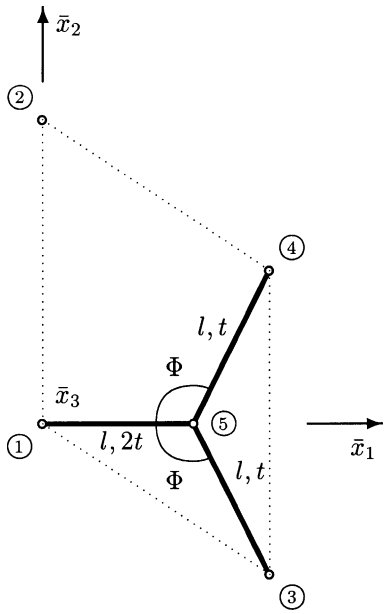

Fig. 8. Hexagonal core – representative volume element.

example. The third example is a more sophisticated FlexCore [1]-type cellular structure, which is common in conjunction with curved sandwich shells.

5.1. Regular hexagonal core

The first geometry to be considered is the well-known regular hexagonal honeycomb core. An appropriate representative volume element for this core geometry is presented in Fig. 8. The coordinates of the nodal points are given in Table 1. Constant length l of all cell walls and a cell wall angle of $\Phi = 120°$ are assumed. Due to the manufacturing process, the cell wall thickness of the cell wall element parallel to the x_1-axis is twice the thickness t of the inclined cell walls. A relative density of $\overline{\rho} = 0.02$ is assumed which is a typical value for a low-density commercial sandwich core. The core thickness is varied from $h = 0$ to $h = 5l$.

[1] FlexCore is a registered Trademark of the Hexcel Corp., Dublin, CA, USA.

Table 1
Hexagonal core – nodal points

i	1	2	3	4	5
$\overline{x}_{(i)1}$	0	0	$\frac{3}{2}l$	$\frac{3}{2}l$	1
$\overline{x}_{(i)2}$	0	$\sqrt{3}l$	$-\frac{3}{2}l$	$\frac{3}{2}l$	0

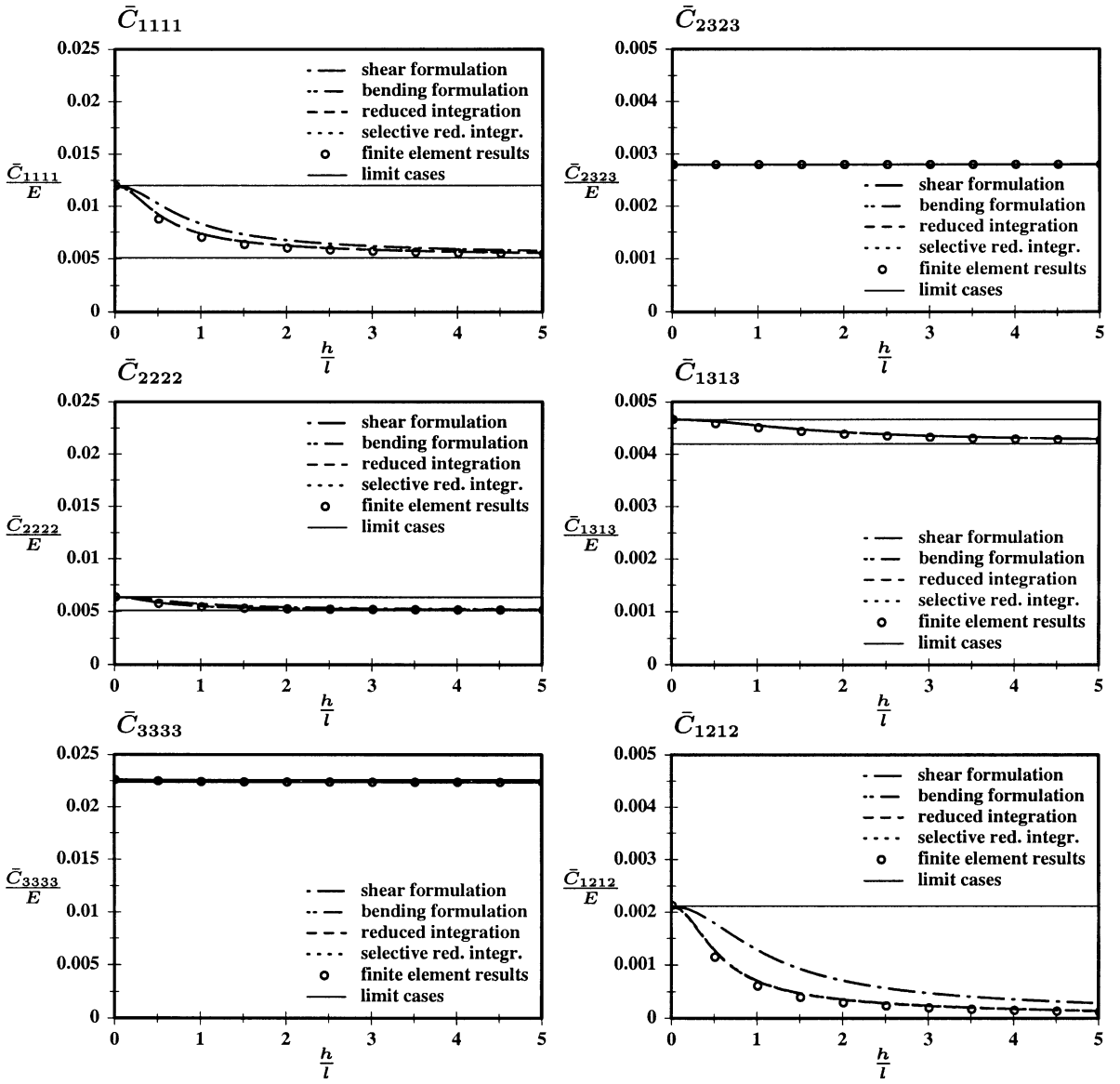

Fig. 9. Hexagonal core – normal and shear components.

In Figs. 9 and 10, the components $\overline{C}_{ijkl}$ of the effective elasticity tensor – normalized by Young's modulus of the cell wall material – are presented in dependence of the normalized core thickness h/l. Components

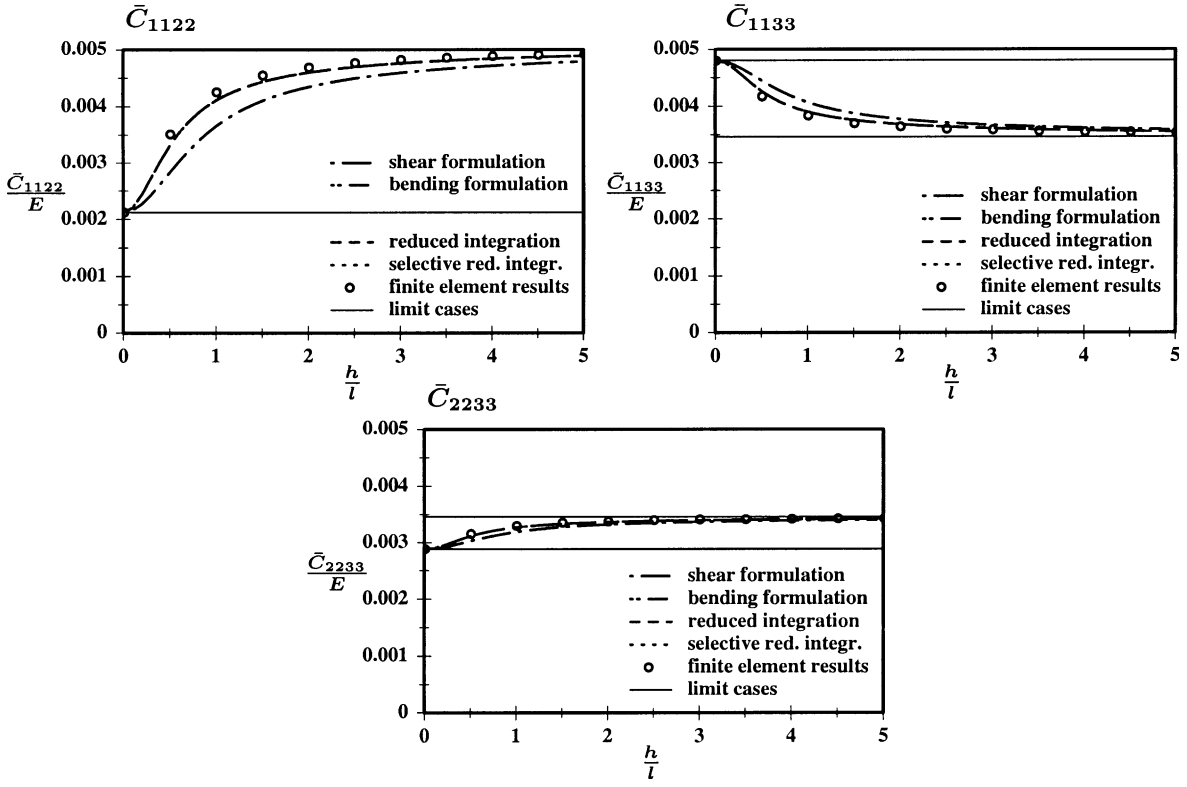

Fig. 10. Hexagonal core – coupling components.

which are not presented in Figs. 9 and 10 are identical to zero due to the orthotropy of the regular hexagonal core. Especially in case of the in-plane normal and shear properties $\overline{C}_{1111}$, $\overline{C}_{2222}$ and $\overline{C}_{1212}$ as well as the in-plane coupling component $\overline{C}_{1122}$, a strong variation of the effective properties with the core thickness is observed. This effect is caused by the variation of the contribution of the transition zones to the total strain energy in the representative volume element with varying core thickness h. Since it causes a thickness dependence of the effective properties, the core face sheet constraint effect has been termed "thickness effect" in the literature (Becker, 1998).

In a comparison of the bending formulation (23)–(25) with full analytical integration to the simplified approaches with reduced integration (26)–(28) and selective reduced integration (29)–(31), the results of all three approaches are found to be almost identical. Thus, the simplified approaches with reduced and selective reduced integration yield adequate results in this low-density example. A good agreement with the numerical reference solution is observed.

The results based on the analytical analyses are slightly larger than the numerical results in all cases, where the stiffness of the perfectly constrained core is larger than the stiffness of the unconstrained core. Slightly lower values are obtained in case of $\overline{C}_{2233}$ and $\overline{C}_{1122}$, where the stiffness of the unconstrained core is larger than the stiffness of the perfectly constrained core due to the large in-plane Poisson's ratio of the regular hexagonal honeycomb core (Gibson and Ashby, 1997).

The agreement of the analytical and numerical approaches is worse in case of the generalization (18)–(20) of the shear formulation of Becker (1998). Thus, the enhancement of the assumption for the dis-

Table 2
Hexagonal core – decay parameter

	$\overline{\varepsilon}_{11}$	$\overline{\varepsilon}_{22}$	$\overline{\varepsilon}_{33}$	$\overline{\varepsilon}_{23}$	$\overline{\varepsilon}_{13}$	$\overline{\varepsilon}_{12}$
$\overline{\varepsilon}_{11}$	3.006	3.009	3.007	3.006	1.822	2.978
$\overline{\varepsilon}_{22}$		3.002	2.994	3.002	1.245	2.962
$\overline{\varepsilon}_{33}$			3.009	3.009	1.054	2.958
$\overline{\varepsilon}_{23}$				–	0.995	2.957
$\overline{\varepsilon}_{13}$					0.995	1.909
$\overline{\varepsilon}_{12}$						2.957

Table 3
Hexagonal core – comparison with the experimental data

Hexcel-code	$l_1 = l_2$ (mm)	$2t_1 = t_2$ (mm)	Hexcel (1987)		Present study	
			G_{13} (MPa)	G_{23} (MPa)	G_{13} (MPa)	G_{23} (MPa)
3/16-5052-.0007	2.8	0.018	186	99	153	100
1/4-5052-.0007	3.7	0.018	144	76	116	76
3/8-5052-.0007	5.5	0.018	83	48	79	51
3/8-5052-.001	5.5	0.025	144	76	110	71
3/8-5052-.002	5.5	0.051	296	146	224	143

placement field to account for cell wall bending with respect to the longitudinal axis in the transition zone improves the results significantly.

The values of the decay parameter λ obtained for the different macroscopic reference strain states are presented in Table 2 for the case of a honeycomb core with $h = l$. Note that for all reference strain states only one or two components of $\overline{\varepsilon}_{ij}$ have non-zero values. It can be observed from Table 2 that in all cases where only normal strains $\overline{\varepsilon}_{11}$, $\overline{\varepsilon}_{22}$ or $\overline{\varepsilon}_{33}$ or in-plane shear deformation $\overline{\varepsilon}_{12}$ are present, a decay parameter of $\lambda \approx 3$ is obtained. Thus, transition zones of approximately equal width are obtained in these cases. If a transverse shear deformation $\overline{\varepsilon}_{13}$ is present, a smaller value of the decay parameter is obtained indicating a lower decay rate of the core face sheet constraint and thus a broader transition zone than in the other cases. No value of λ is given for the case where only $\overline{\varepsilon}_{23}$ has a non-zero value since for this case the upper and lower bound solutions corresponding to the unconstrained and the perfectly constrained core respectively are equal (Fig. 9).

In Table 3, a comparison of the effective transverse shear moduli G_{23} and G_{13} obtained by the present method with experimental data from the catalogue of the Hexcel Corp. (1987) is presented. Five different cases of regular honeycomb cores with a thickness of 15.9 mm are considered. The cell wall material properties are assumed to be $E = 72000$ MPa and $\nu = 0.34$, respectively (aluminium). A good agreement is observed in all the cases under consideration.

5.2. Tubular core

The second example to be considered is a tubular sandwich core with moderate relative density. An appropriate representative volume element for this geometry is presented in Fig. 11. The coordinates of the nodal points are given in Table 4. The mean tube diameter is $2r$. A constant cell wall thickness t is assumed, which is determined in such a way that a relative density $\overline{\rho} = 0.1$ is obtained. The core thickness is varied from $h = 0$ to $h = 10r$.

The results are presented in Fig. 12. Isotropic behaviour of the geometry with respect to the in-plane directions is obtained. Therefore, the in-plane normal components $\overline{C}_{1111}$ and $\overline{C}_{2222}$ are equal as well as the

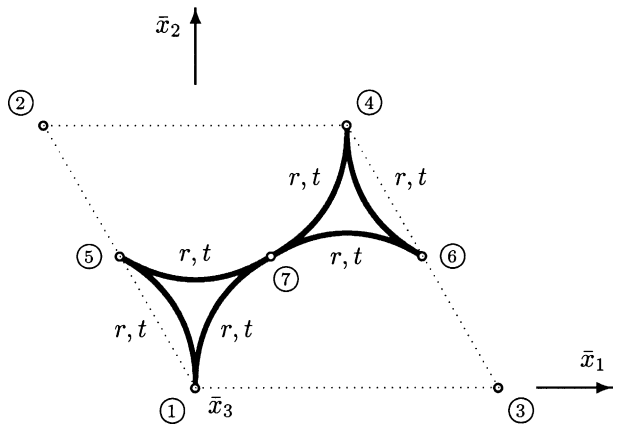

Fig. 11. Tubular core – representative volume element.

Table 4
Tubular core – nodal points

i	1	2	3	4	5	6	7
$\bar{x}_{(i)1}$	0	$-r$	$2r$	r	$-\frac{1}{2}r$	$\frac{3}{2}r$	$\frac{1}{2}r$
$\bar{x}_{(i)2}$	0	$\sqrt{3}r$	0	$\sqrt{3}r$	$\frac{\sqrt{3}}{2}r$	$\frac{\sqrt{3}}{2}r$	$\frac{\sqrt{3}}{2}r$

associated coupling components $\overline{C}_{1133}$ and $\overline{C}_{2233}$ and the transverse shear properties $\overline{C}_{2323}$ and $\overline{C}_{1313}$. No in-plane normal-shear coupling as well as transverse shear coupling is present.

Again, a strong effect of the core thickness on the effective in-plane normal and shear properties $\overline{C}_{1111}$, $\overline{C}_{2222}$ and $\overline{C}_{1212}$ as well as the normal coupling components $\overline{C}_{2233}$, $\overline{C}_{1133}$ and $\overline{C}_{1122}$ is observed. The effect is caused by the transition in the mode of deformation from pure cell wall bending in case of the unconstrained core to pure cell wall stretching in case of the perfectly constrained core.

As in case of the low-density hexagonal core, a rather good agreement of the bending formulation (23)–(25) and the finite element based reference solution is obtained. In contrast to the low-density hexagonal core considered in Section 5.1, the excellent agreement of the results based on the reduced and selective reduced integration schemes with the results based on the full analytical integration scheme is not observed in the present example. Since the assumption of small cell wall thickness t is not satisfied in case of the moderate density core, the good agreement observed in Section 5.1 is lost in the present example. It is clearly observed that the results based on the reduced integration scheme (26)–(28) fail to approach the limit case of the unconstrained core in the thick core limit ($h \to \infty$), while the results based on the selective reduced integration scheme (29)–(31) do approach this limit case. Nevertheless, in most cases, the agreement of the selective reduced and the full analytical integration scheme is still reasonable although the requirement $t \ll l, h$ for application of the reduced integration schemes is not satisfied.

The shear formulation (18)–(20) yields results which are much larger than the reference solution. Since in the underlying assumption (16) for the displacement field it is assumed that the transition from the mode of deformation associated with the unconstrained core to the mode of deformation of the face sheets occurs by pure shear deformation, the bending mode with respect to the longitudinal axis is suppressed. The shear mode for the transition is associated with larger strain energy values than the bending mode. Hence, the total strain energy and subsequently the components of the effective elasticity tensor are overestimated.

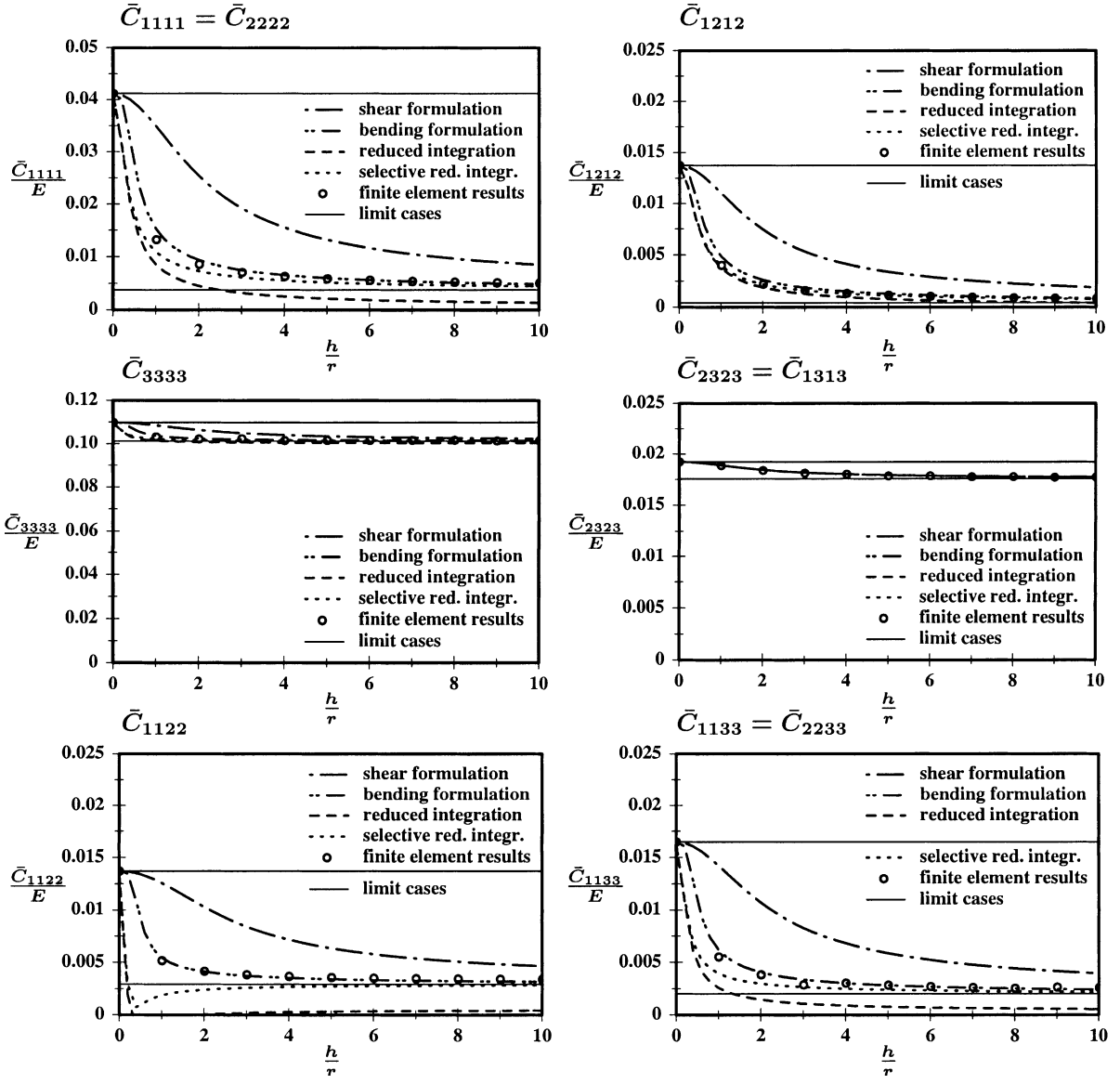

Fig. 12. Tubular core – normal, shear and coupling components.

5.3. FlexCore-type cellular structure

A more complex core geometry is the FlexCore-type cellular structure, which is common in conjunction with strongly curved sandwich shells. An appropriate representative volume element for this type of cellular sandwich core is presented in Fig. 13. The coordinates of the nodal points assumed in this analysis are given in Table 5. A relative density of $\overline{\rho} = 0.05$ is considered by an appropriate choice of the cell wall thickness t. Due to the manufacturing process by adhesive bonding of corrugated sheets, the cell wall elements connecting nodes 3 and 5 as well as nodes 4 and 9 (Fig. 13) are twice as thick as the remaining cell wall elements with thickness t. The core thickness h is varied from 0 to 20 mm.

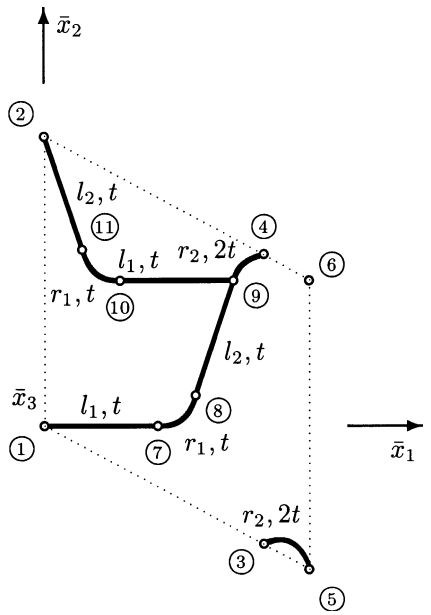

Fig. 13. FlexCore – representative volume element.

Table 5
FlexCore – nodal points

i	1	2	3	4	5	6	7	8	9	10	11
$\bar{x}_{(i)1}$ (mm)	0.00	0.00	5.50	5.50	6.47	6.47	2.70	3.66	4.54	0.87	1.84
$\bar{x}_{(i)2}$ (mm)	0.00	8.00	−3.26	4.74	−4.00	4.00	0.00	0.74	4.00	4.74	4.00

The normalized components $\overline{C}_{ijkl}$ of the effective elasticity tensor for the FlexCore-type structure are presented in Figs. 14 and 15, respectively. A rather strong effect of the core thickness on the effective in-plane properties $\overline{C}_{1111}$, $\overline{C}_{2222}$ and $\overline{C}_{1212}$ and the associated coupling components $\overline{C}_{2233}$, $\overline{C}_{1133}$ and $\overline{C}_{1122}$ is observed. In the thick core limit $h \to \infty$, all of these properties turn out to be small since this core geometry is designed to an outstanding flexibility according to bending with respect to axes in the sandwich plane. On the other hand, relatively large values of the in-plane properties are obtained in the thin core limit ($h \to 0$). In contrast to the geometries considered in Sections 5.1 and 5.2, the effect of the core thickness on the effective properties is also significant in case of the transverse shear properties $\overline{C}_{2323}$ and $\overline{C}_{1313}$ for the present example.

As in the case of the low-density hexagonal honeycomb core, the results based on the bending formulation with full analytical integration (23)–(25) and the results based on the reduced integration scheme (26)–(28) as well as the selective reduced integration scheme (29)–(31) are almost identical. The shear formulation (18)–(20) again overestimates the components of the effective elasticity tensor.

Comparison of the analytical results based on the bending formulation and the numerical reference solution yields a reasonable agreement. Nevertheless, in case of the in-plane normal component $\overline{C}_{1111}$ as well as for the associated coupling components $\overline{C}_{1133}$ and $\overline{C}_{1122}$, a significant deviation of the analytical and numerical results is observed. In the macroscopic reference strain state $\bar{\varepsilon}_{11} \neq 0$, from which $\overline{C}_{1111}$ is de-

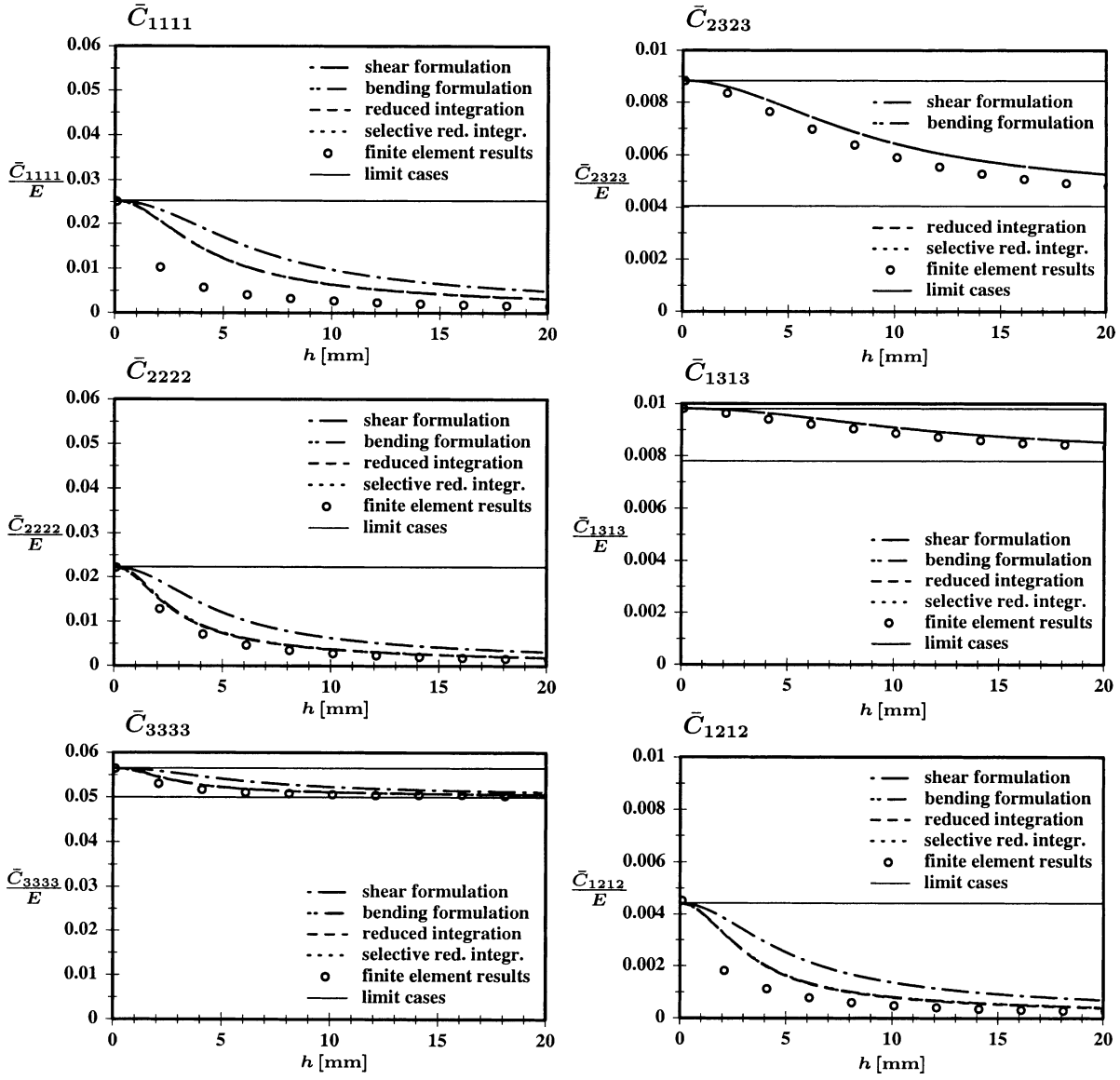

Fig. 14. FlexCore – normal and shear components.

termined (Eq. (5)), the cell walls 1–7 and 9–10 contain the largest fractions of the total strain energy in the entire representative volume element. Therefore, these cell walls dominate in the total strain energy for the reference strain state $\bar{\varepsilon}_{11} \neq 0$. Nevertheless, the deformed configuration of these cell wall elements in the case $\bar{\varepsilon}_{11} \neq 0$ is rather complex especially in the transition zone.

The deformed configurations for six basic reference strain states with only one non-zero effective strain component are presented in Fig. 16. A core thickness of $h = 10$ mm has been assumed. For reasons of a more distinct presentation, cell wall 3–5 has been moved between the cell wall intersections 4 and 6 in this figure. The displacements have been increased by a magnification factor of 150 for the reference strain states

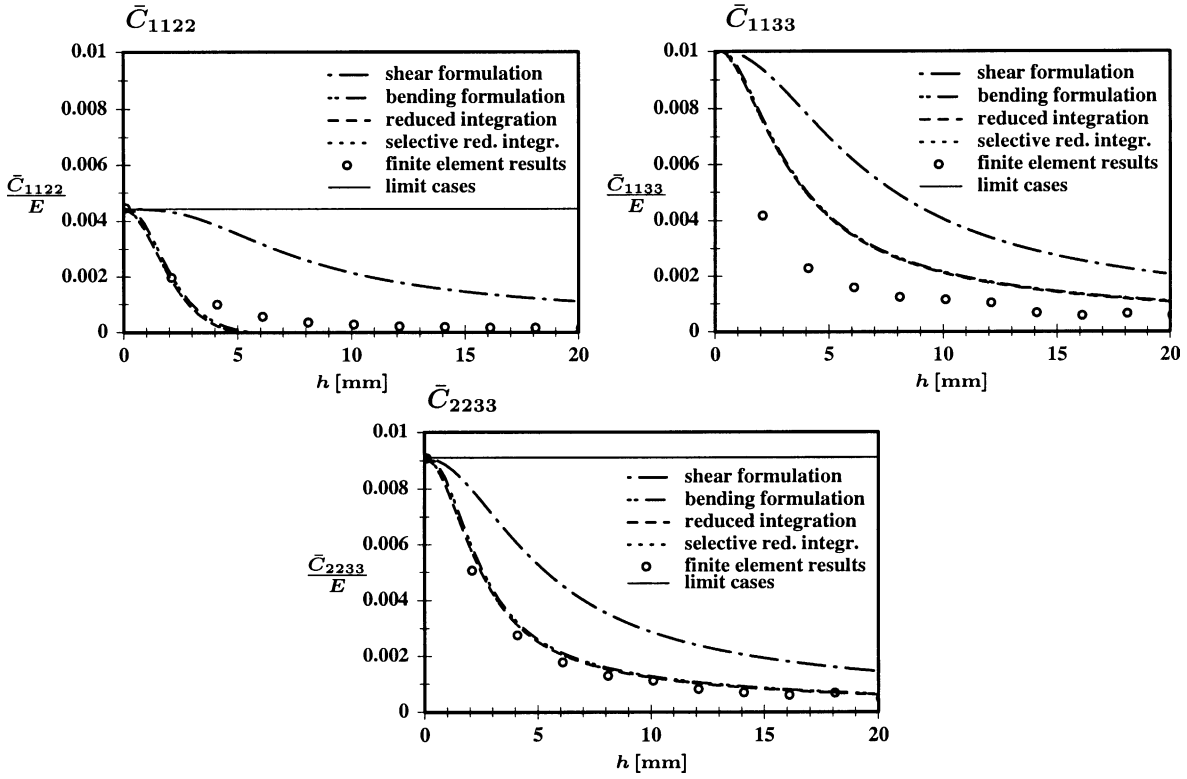

Fig. 15. FlexCore – coupling components.

$\bar{\varepsilon}_{11}$, $\bar{\varepsilon}_{22}$ and $\bar{\varepsilon}_{33}$, while a magnification factor of 75 has been used for the reference strain states $\bar{\varepsilon}_{23}$, $\bar{\varepsilon}_{13}$ and $\bar{\varepsilon}_{12}$. It can be observed that the right end of cell wall element 1–7 is connected to the curved cell wall element 7–8. At the connection to cell wall 1–7, this cell wall, due to its curvature, is relatively stiff with respect to deformation in the $\bar{x}_1$-direction but weak with respect to deformation in the $\bar{x}_2$-direction. The opposite stiffness ratio is present at the other end of cell wall 1–7. Thus, the strain state in the transition zone of cell wall 1–7 involves shear deformation within the cell wall plane, which is distributed non-symmetrically with respect to the centre of the cell wall element. Moreover, non-homogeneously distributed bending deformation with respect to the cell wall longitudinal direction occurs (Fig. 16).

The decay rate of these two types of perturbation to the mode of deformation associated with the unconstrained core is significantly different. Therefore, the assumption that the transition from the mode of deformation associated with the face sheets to the mode of deformation of the unconstrained core could be described by a single parameter λ (in conjunction with the lateral displacements Δu_i) is not valid in cases where more complex displacement fields are present and the total strain energy associated with the different mechanisms of transition is in the same order of magnitude.

Nevertheless, even in this case, the analytical results still define rigorous Voigt type bounds for the elastic moduli and thus for the normal and shear components of the effective elasticity tensor. In addition, it should be noted that the analytical schemes work quite well in the present example, when the transverse shear properties $\overline{C}_{2323}$ and $\overline{C}_{1313}$ as well as the transverse normal component $\overline{C}_{3333}$ are considered. From the technological point of view, these are the most important properties since within the principle of sandwich construction, the core has to carry the transverse shear and normal loads.

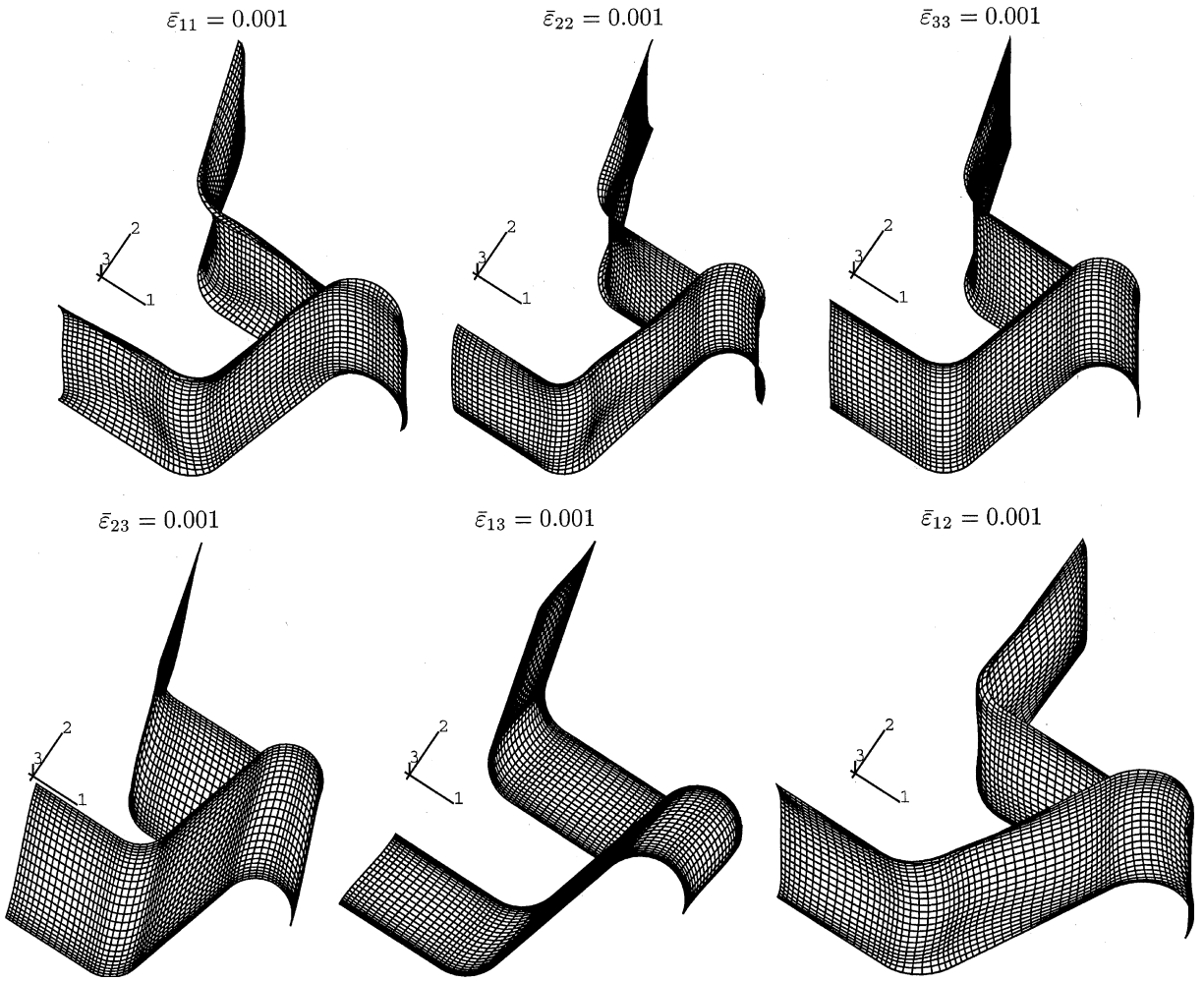

Fig. 16. FlexCore – deformed configuration.

6. Conclusions

The aim of this study is the analysis of the effective elasticity tensor for two-dimensional cellular sandwich cores with general cell geometry in consideration of constraints due to the incompatibility of the mode of deformation associated with the face sheets and the mode of deformation associated with the unconstrained core. The determination of the components of the effective elasticity tensor is performed by means of a strain energy based RVE concept, which has been developed in an earlier study. This concept assumes equivalence of the mechanical behaviour of a representative volume element for the given microstructure and a similar volume element consisting of the effective medium, if equal strain energy in both volume elements is caused by strain states which are equal in a volume average sense.

For evaluation of the strain energy, a displacement field for the individual cell walls is proposed which is compatible with the deformation of the face sheets. The compatible displacement field is determined by means of a weighted superposition of the displacement field of the unconstrained core and an extension of

the displacement field of the face sheets into the core region. Within this concept, the weight function depends on the distance to the face sheets. A free parameter within the weight function is determined by application of the principle of minimum strain energy. Since the analytical concept is based on kinematically admissible displacement and strain fields in conjunction with the principle of minimum strain energy, the values obtained for the normal and shear components of the effective elasticity tensor define rigorous Voigt type bounds. Nevertheless, in many cases especially for standard commercial sandwich cores, the obtained bounds could be expected close to the actual values of the properties under consideration.

The analytical concept is applied to the analysis of three different commercial sandwich core geometries, where examples with low and moderate relative density and straight as well as curved cell walls are considered. Four different formulations of the analytical scheme are compared to a reference solution which is obtained numerically by means of the finite element method. In all cases, a significant dependence of the effective properties on the core thickness is observed. This effect can be explained by the variation of the contribution of the transition zone to the total strain energy of the entire representative volume element with varying core thickness.

The first formulation of the analytical scheme is based on the assumption that the mechanism of transition in the modes of deformation consists of pure shear deformation. This approach is found to overestimate the strain energy especially in case of thick cell walls. A second approach assumes that cell wall bending is the dominant mechanism of the transition in deformation modes. Results based on this approach are found close to the reference results except in one case regarding the in-plane properties of FlexCore-type cellular material. Since the second approach yields rather lengthy equations, two simplified versions are derived. In case of low-density cores, the results of the simplified and original versions are found to be almost identical, while some deviations are observed in an example with moderate relative density. Nevertheless, in contrast to the first two approaches, the simplified approaches do not define rigorous bounds for the effective properties since terms in the expressions of the strain energy have been neglected.

Advantage of the present method for analysis of the effective properties of cellular sandwich cores is the fact that all components of the effective elasticity tensor are directly accessible. No restrictions with respect to the cell geometry apply. Finally, the outstanding numerical efficiency of the analytical approaches compared to the finite element analysis should be emphasized.

Acknowledgements

This work was financially supported by the Deutsche Forschungsgemeinschaft (DFG, German Research Association) under Grant No. Be 1090/4-1.

Appendix A. Generalized displacement vectors and matrices

A.1. Unconstrained core

The generalized nodal deflection vectors and corresponding matrices for the free, unconstrained core according to Eq. (7) are given by

$$[\tilde{v}_1^{\mathrm{f}}] = \begin{pmatrix} \frac{\bar{v}^{\mathrm{f}}_{(1)1}}{l} \\ \frac{\bar{v}^{\mathrm{f}}_{(2)1}}{l} \\ \bar{\varepsilon}_{33} \end{pmatrix}, \qquad [M_1] = \begin{pmatrix} 1 & -1 & -\nu \\ -1 & 1 & \nu \\ -\nu & \nu & 1 \end{pmatrix}, \tag{A.1}$$

$$[\tilde{v}_2^{\mathrm{f}}] = \begin{pmatrix} \frac{\tilde{v}^{\mathrm{f}}_{(1)2}}{l} \\ \Delta\tilde{\varphi}_{(1)} \\ \frac{\tilde{v}^{\mathrm{f}}_{(2)2}}{l} \\ \Delta\tilde{\varphi}_{(2)} \end{pmatrix}, \qquad [M_2] = \begin{pmatrix} 1 & \frac{1}{2} & -1 & \frac{1}{2} \\ \frac{1}{2} & \frac{1}{4} & -\frac{1}{2} & \frac{1}{4} \\ -1 & -\frac{1}{2} & 1 & -\frac{1}{2} \\ \frac{1}{2} & \frac{1}{4} & -\frac{1}{2} & \frac{1}{4} \end{pmatrix}, \tag{A.2}$$

$$[\Delta\tilde{\varphi}] = \begin{pmatrix} \Delta\tilde{\varphi}_{(1)} \\ \Delta\tilde{\varphi}_{(2)} \end{pmatrix}, \qquad [M_\varphi] = \begin{pmatrix} 1 & -1 \\ -1 & 1 \end{pmatrix}, \tag{A.3}$$

$$[\tilde{v}_3^{\mathrm{f}}] = \begin{pmatrix} \frac{\tilde{v}^{\mathrm{f}}_{(1)3}}{l} \\ \frac{\tilde{v}^{\mathrm{f}}_{(2)3}}{l} \end{pmatrix}, \qquad [M_3] = \begin{pmatrix} 1 & -1 \\ -1 & 1 \end{pmatrix}. \tag{A.4}$$

A.2. Perfectly constrained core

The generalized nodal deflection vectors for the perfectly constrained core according to Eq. (14) are given by

$$[\tilde{v}_1^{\mathrm{c}}] = \begin{pmatrix} \frac{\tilde{v}^{\mathrm{c}}_{(1)1}}{l} \\ \frac{\tilde{v}^{\mathrm{c}}_{(2)1}}{l} \\ 0 \end{pmatrix}, \qquad [\tilde{v}_2^{\mathrm{c}}] = \begin{pmatrix} \frac{\tilde{v}^{\mathrm{c}}_{(1)2}}{l} \\ 0 \\ \frac{\tilde{v}^{\mathrm{c}}_{(2)2}}{l} \\ 0 \end{pmatrix}, \qquad [\tilde{v}_3^{\mathrm{c}}] = \begin{pmatrix} \frac{\tilde{v}^{\mathrm{c}}_{(1)3}}{l} \\ \frac{\tilde{v}^{\mathrm{c}}_{(2)3}}{l} \end{pmatrix}. \tag{A.5}$$

A.3. Coupling terms

The generalized nodal deflection vectors and corresponding matrices for the coupling terms are given by

$$[\tilde{v}_1^{\mathrm{c}*}] = \begin{pmatrix} \frac{\tilde{v}^{\mathrm{c}}_{(1)1}}{l} \\ \frac{\tilde{v}^{\mathrm{c}}_{(2)1}}{l} \\ 0 \end{pmatrix}, \qquad [\tilde{v}_1^{\mathrm{f}*}] = \begin{pmatrix} \frac{\tilde{v}^{\mathrm{f}}_{(1)1}}{l} \\ \frac{\tilde{v}^{\mathrm{f}}_{(2)1}}{l} \\ 0 \end{pmatrix}, \tag{A.6}$$

$$[M_2^*] = \begin{pmatrix} 1 & 0 & -1 & 0 \\ 0 & -\frac{1}{4} & 0 & -\frac{1}{4} \\ -1 & 0 & 1 & 0 \\ 0 & -\frac{1}{4} & 0 & -\frac{1}{4} \end{pmatrix}, \tag{A.7}$$

$$[M_\varphi^*] = \begin{pmatrix} 1 & \frac{1}{2} \\ \frac{1}{2} & 1 \end{pmatrix}, \tag{A.8}$$

$$[\tilde{v}_1^{\mathrm{a}}] = \begin{pmatrix} \frac{\tilde{v}^{\mathrm{c}}_{(1)1}}{l} \\ \frac{\tilde{v}^{\mathrm{c}}_{(2)1}}{l} \\ \frac{\tilde{v}^{\mathrm{f}}_{(1)1}}{l} \\ 0 \\ \frac{\tilde{v}^{\mathrm{f}}_{(2)1}}{l} \\ 0 \\ \frac{\Delta\tilde{u}_1}{l} \end{pmatrix}, \qquad [\tilde{v}_2^{\mathrm{a}}] = \begin{pmatrix} \frac{\tilde{v}^{\mathrm{c}}_{(1)2}}{l} \\ \frac{\tilde{v}^{\mathrm{c}}_{(2)2}}{l} \\ \frac{\tilde{v}^{\mathrm{f}}_{(1)2}}{l} \\ \Delta\tilde{\varphi}_{(1)} \\ \frac{\tilde{v}^{\mathrm{f}}_{(2)2}}{l} \\ \Delta\tilde{\varphi}_{(2)} \\ \frac{\Delta\tilde{u}_2}{l} \end{pmatrix}, \qquad [\Delta\tilde{\varphi}^{\mathrm{a}}] = \begin{pmatrix} 0 \\ 0 \\ 0 \\ \Delta\tilde{\varphi}_{(1)} \\ 0 \\ \Delta\tilde{\varphi}_{(2)} \\ 0 \end{pmatrix}, \qquad [\tilde{v}_3^{\mathrm{a}}] = \begin{pmatrix} \frac{\tilde{v}^{\mathrm{c}}_{(1)3}}{l} \\ \frac{\tilde{v}^{\mathrm{c}}_{(2)3}}{l} \\ \frac{\tilde{v}^{\mathrm{f}}_{(1)3}}{l} \\ 0 \\ \frac{\tilde{v}^{\mathrm{f}}_{(2)3}}{l} \\ 0 \\ \frac{\Delta\tilde{u}_3}{l} \end{pmatrix} \tag{A.9}$$

$$[M_{\mathrm{a}}] = \begin{pmatrix} 1 & \frac{1}{2} & -1 & -\frac{1}{8} & -\frac{1}{2} & \frac{1}{8} & \frac{3}{2} \\ \frac{1}{2} & 1 & -\frac{1}{2} & -\frac{1}{8} & -1 & \frac{1}{8} & \frac{3}{2} \\ -1 & -\frac{1}{2} & 1 & \frac{1}{8} & \frac{1}{2} & -\frac{1}{8} & -\frac{3}{2} \\ -\frac{1}{8} & -\frac{1}{8} & \frac{1}{8} & \frac{1}{40} & \frac{1}{8} & -\frac{1}{40} & -\frac{1}{4} \\ -\frac{1}{2} & -1 & \frac{1}{2} & \frac{1}{8} & 1 & -\frac{1}{8} & -\frac{3}{2} \\ \frac{1}{8} & \frac{1}{8} & -\frac{1}{8} & -\frac{1}{40} & -\frac{1}{8} & \frac{1}{40} & \frac{1}{4} \\ \frac{3}{2} & \frac{3}{2} & -\frac{3}{2} & -\frac{1}{4} & -\frac{3}{2} & \frac{1}{4} & 3 \end{pmatrix}. \tag{A.10}$$

References

Bakhvalov, N.S., Panasenko, G., 1989. Homogenization: Averaging Processes in Periodic Media. Kluwer Academic Publishers, Dordrecht.

Becker, W., 1998. The inplane stiffness of a honeycomb core including the thickness effect. Archive of Applied Mechanics 68, 334–341.

Bishop, J.F.W., Hill, R., 1951. A theory of the plastic distortion of a polycrystalline aggregate under combined stress. Philosophical Magazine 42, 414–427.

Chang, C.C., Ebcioglu, I.K., 1961. Effect of cell geometry on the shear modulus and on density of sandwich panel cores. Journal of Basic Engineering 83, 513–518.

Gibson, L.J., Ashby, M.F., Schajer, G.S., Robertson, C.I., 1982. The mechanics of two-dimensional cellular materials. Proceedings of the Royal Society A382, 25–42.

Gibson, L.J., Ashby, M.F., 1997. Cellular Solids. Structure and Properties. Cambridge University Press, Cambridge.

Grediac, M., 1993. A finite element study of the transverse shear in honeycomb cores. International Journal of Solids and Structures 30, 1777–1788.

Hashin, Z., Shtrikman, S., 1962. A variational approach to the theory of the elastic behaviour of polycrystals. Journal of the Mechanics and Physics of Solids 10, 343–352.

Hexcel Corp., 1987. Mechanical Properties of Hexcel Honeycomb Materials, TSB120. Hexcel Corp. Dublin, CA.

Hill, R., 1952. The elastic behaviour of a crystalline aggregate. Proceedings of the Royal Society A65, 349–354.

Hill, R., 1984. On macroscopic effects of heterogenity in elastoplastic media at finite strain. Mathematical Proceedings of the Cambridge Philosophical Society 95, 481–494.

Hohe, J., Becker, W., 1999. Effective elastic properties of triangular grid structures. Composite Structures 45, 131–145.

Hohe, J., Becker, W., 2000. An energetic homogenization procedure for the elastic properties of general cellular sandwich cores. Composites B, in press.

Kelsey, S., Gellatley, R.A., Clark, B.W., 1958. The shear modulus of foil honeycomb cores. Aircraft Engineering 30, 294–302.

Meraghni, F., Desrumaux, F., Benzeggagh, M.L., 1999. Mechanical behaviour of cellular core for structural sandwich panels. Composites A30, 767–779.

Castaneda, P., Suquet, P., 1998. Nonlinear composites. Advances in Applied Mechanics 34, 171–302.

Sanchez-Palencia, E., 1980. Non-Homogeneous Media and Vibration Theory. Springer, Berlin.

Torquato, S., Gibianski, L.V., Silva, M.J., Gibson, L.J., 1998. Effective mechanical and transport properties of cellular solids. International Journal of the Mechanical Sciences 40, 71–82.

Voigt, W., 1889. Ueber die Beziehung zwischen den beiden Elasticitätsconstanten isotroper Körper. Annalen der Physik und Chemie 274, 573–587 (in German).

Warren, W.E., Kraynik, A.M., 1987. Foam mechanics: The linear elastic response of two-dimensional spatially periodic cellular materials. Mechanics of Materials 6, 27–37.